Theoretical Analysis of Biomolecules Using BSM models

S. Sarg

Abstract One of the amazing features of the biomolecules is their ability to preserve their own three-dimensional shape in proper environments. This effect can not obtain satisfactory theoretical explanation from a point of view of the quantum mechanical models of the atoms. These models are based on the planetary concept where the nuclear size is a few order smaller than the average size of the orbits. Additionally, the uncertainty principle on which the quantum mechanical models rely, does not show its signature in the complex structure and deterministic behaviour of the biomolecules. A recent interdisciplinary study from different fields of physics and chemistry indicates that the real atoms are different from the planetary atomic models. This difference is not from energetic, but from a structural aspect. A recently developed unified theory called Basic Structures of Matter (BSM), based on a new concept about the vacuum space, allowed unveiling of the real physical structures of the atoms. The obtained physical models exhibit the same energetic levels as the quantum mechanical models, while possessing, in the same time, nuclear structures quite different from the nuclei in the planetary atomic models. They allows to study the physical conditions behind the structural and bond restrictions of the atoms connected in molecules. The existing data base about the structure and atomic composition of the organic and biomolecules, provides an excellent opportunity for reliable validation of the suggested physical models of the atoms. The current work includes a brief introduction to the BSM theory and demonstration of a new method for theoretical analysis of biomolecules using BSM models. Such method applied for analysis of DNA and tRNA molecules led to formulation of two hypotheses: for energy storage mechanism in proteins and for DNA involvement in a cell cycle synchronization.

Keywords: *Molecular biology, structure of biomolecules, Structural chemistry, biophysics, biochemistry, VSEPR model, proteins, DNA research, C-value paradox, Levinthal's paradox,*

1. Introduction

Despite the huge number of possible configurations of the atoms in the proteins, according to the Quantum mechanics, they fold reliably and quickly to their native state. This effect is known in the biochemistry as a Levinthal's paradox. If considering only the Quantum mechanical considerations a protein molecule from 2,000 atoms, for example should possess an astronomical number of degrees of freedom. It is known, however, that this number is drastically reduced by some strong structural restrictions, such as bond lengths, relative bond angles and rotations. The complex secondary and tertiary structures of the biomolecules provide indications of additional restrictions with weaker strength but responsible for their complex shapes. All this restrictions could not get satisfactory explanation by the Quantum mechanical models of the atoms. While these models rely heavily on the uncertainty principle, the quite deterministic structure and behaviour of complex molecules like proteins do not show its signature.

Interdisciplinary studies from different fields of physics indicate that the Quantum mechanical models of the atoms are rather mathematical models than physical, so they are not able to provide all the features of the real atoms. Such studies led to development of original unified field theory called Basic Structures of Matter (BSM). Based on a new concept about the vacuum space, BSM theory allowed unveiling the physical structures of the atoms. The nuclei, in the obtained physical models, provide structural and angular restrictions on the chemical bonds. In the same time, the physical models of the atoms possess the same energy levels and interaction properties as the quantum mechanical models.

The purpose of the initial part of this article (from section 2 to section 10) is to acquaint the scientist from the field of molecular biology with the concept of the BSM theory and particularly with physical models of the atoms. The second part of the article (from section 11.1 to section 12.2) shows applications of a new analytical approach for studying the properties of the biomolecules. The application of this approach resulted in formulation of two hypotheses: for energy storage mechanism in proteins and for a possible involvement of eukariotic DNA in a cell cycle synchronization.

2. The new point of view of the BSM theory

A new theoretical study, provided by BSM theory, indicates that the vacuum is not a void space, but possessing a underlying grid structure of

superdense particles. Extensive analysis of phenomena from different fields of physics allowed to formulate the search criteria for the possible physical model of this structure. Its properties must explain the basic physical effects in the complex "matter - energy - space - time - gravitation - fields". As a result, one of the most promising model is suggested. It allows successful analysis of different type of physical phenomena from a new point of view.

According to the suggested model, the vacuum space possesses a underlying diamond shape grid structure of sub-elementary particles arranged in nodes. These particles called twisted prisms are formed of two types super dens intrinsic matter substances. Prisms of the same type are attracted in a pure void space by Intrinsic Gravitational (IG) forces that are inverse proportional to a cube of the distance. Every node is comprised of four prisms held by IG forces, so, its geometry is flexible. The prisms possess axial IG anisotropy with a twisting component, due to a lower level structure. They are called twisted prisms. The IG field is a type of energy interaction between intrinsic matter at lower level of matter organization involved in an intrinsic energy balance. The gaps between the alternatively arranged nodes of different types are also results of an intrinsic energy balance. The estimated distance between neighbouring nodes of the grid is in order of $(1 \sim 2)E-20$ (m), while the matter density of the prisms is about 1E13 times higher than the density of the average atomic matter. This structure fills all the visible volume of the Universe. It is called a Cosmic Lattice (CL), so the vacuum in BSM theory is referenced as a CL space.

The new concept broadens our vision about the space-time and matter-energy relations. Using the vacuum grid as a frame of reference, the BSM theory allows to separate the space from time parameters at a low level of matter organization and to perform physical analysis in a real three dimensional space. In such approach the quantum mechanical rules and the relativistic phenomena are completely understandable and explainable by the human logic without a need of the uncertainty principle.

The self-sustainable CL structure is supported by super strong interactions between the highly dens intrinsic matter from which the prisms are built. In the same time, the node distance is very weakly influenced by the atomic matter of massive astronomical objects. This effect is quite weak because for the range of CL node distance the Newtonian gravitation is negligible in comparison to the Intrinsic Gravitation. While the node distance is about 10E9 times smaller than the average internuclear distance of the atoms in a solids body, the matter density in the prisms is about 1E13 times higher than the average atomic matter. Therefore, the massive astronomical objects are able to hold CL space. This defines the local conditions of the light velocity, while the gradient of slightly affected node distance defines the General relativistic conditions.

Another specific feature of the CL space is the ability of the CL nodes to fold and pass through the grid structure of a normal CL space when a less massive object moves in a CL space of a more massive one. Such unique feature does not have counterpart in any concept of aether or ideal fluid. In the same time, it is closely related to the inertial properties of the atomic matter in CL space and the equivalence between gravitational and inertial mass.

By analysis of the dynamics and mutual interactions of the CL nodes (§2.9 of BSM), it is possible to understand some of fundamental physical parameters, such as: unite charge, magnetic field, Planck constant, Zero Point Energy, photon wavetrain structure, light velocity, permeability and permittivity of vacuum. The CL node has two sets of symmetrical axes: one set of 4 axes along anyone of the prisms called *abcd* axes, and another set of 3 orthogonal axes called *xyz* axes. The orthogonal *xyz* axes of the neighbouring CL nodes are aligned. Such arrangement gives conditions for complex node oscillations under the inverse cubic law of intrinsic gravitation. The deviated from the central position CL node exhibits set of minimums that can be associated with energy wells. **Two symmetrical minimums appear along anyone of *xyz* axes and one minimum along the positive direction of anyone of *abcd* axes.** These set of minimums provide the total energy well of CL node (Zero Point Energy of vacuum) from one side and conditions for complex oscillations from the other. Fig. [2.24] illustrates the return forces along the two sets of axes and the associated with them energy wells. The

right vertical axis indicates specific energy points. The energy level E_{C2} corresponds to the filled energy wells or the Zero Point Energy of the vacuum.
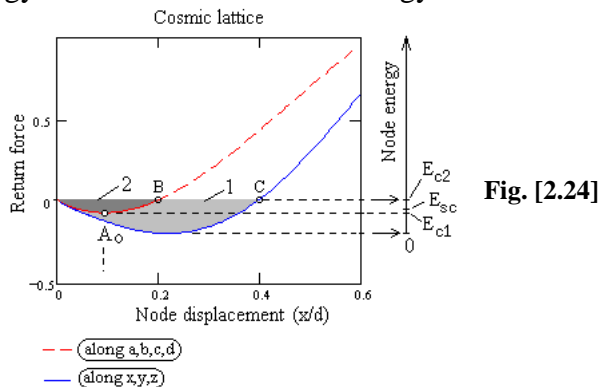

Fig. [2.24]

The complex CL node oscillations are characterised by two types of cycles: a resonance cycle and a SPM cycle (the latter is described by a Spatial Precession Momentum vector). The trace of the resonance cycle is approximately flat but open curve with four bumps, as shown in Fig. [2.26] The points A and B from the resonance cycle are pretty close but not coinciding, so the segment AB with a finite length is align almost at 90 deg in respect to the drawing plane.
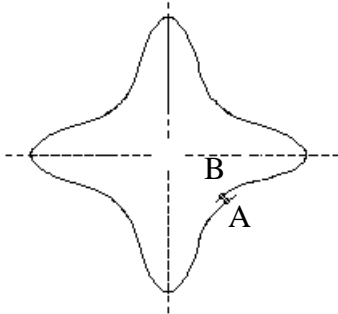

Fig. [2.26]

The lack of coincidence between any initial (A) and final (B) point from one resonance cycle is a result of the asymmetrical spatial positions of the energy wells in respect to the central node point (node point for zero deviation). The average plane of the resonance trace is slightly rotated with every cycle, so after a large number of such cycles the node trace passes through the same (arbitrary selected) initial point A. This is a SPM cycle. The number of the resonance cycle in one SPM cycle, estimated in BSM, is $N_{RQ} = 0.88431155 \times 10^9$. The the tip of SPM vector for one full cycle circumscribes a closed surface with central point symmetry and six bumps aligned along the axes xyz. Such type of surface is referenced in BSM as a Quasisphere. It is

found that the resonance cycle is related to the velocity of the energy wave propagation (light velocity), while the SPM cycle is related to quantum features of the CL space. In such conditions, the SPM cycle is responsible for the constant light velocity, due to the quantum properties of the SPM quasispheres and their mutual interactions. The frequency of SPM cycle is equal to the known Compton frequency. In absence of any electrical charge, the SPM Quasisphere possesses a central point of symmetry and it is called a Magnetic Quasisphere (MQ). This is a normal state of the oscillating CL node that appears to be related to the magnetic permeability of the vacuum. In presence of electrical charge, the SPM quasisphere obtains a deformation as an elongation along its diameter connecting two opposite bumps, and it is called an Electrical Quasisphere (EQ). The shapes of MQ and EQ are shown in Fig. 1.
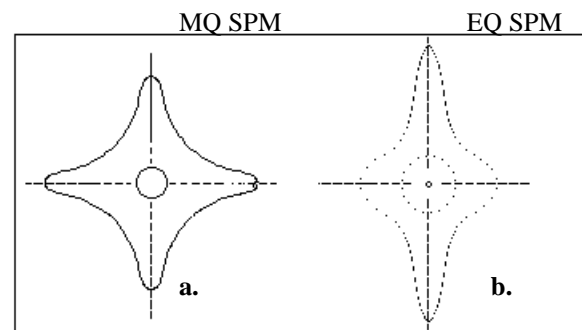

Fig. 1 MQ and EQ of SPM

The electrical field is composed of spatially oriented and synchronized EQ nodes.

The magnetic field is a closed loop in the CL space involving only MQ type of nodes whose SPM frequencies are synchronized. Such arrangement, however, has some specific spatial and temporally features:

- The CL nodes of right handed prisms are commonly synchronized

- The CL nodes of the left-handed prisms are commonly synchronized

- The phase difference between the involved left and right handed nodes determines the direction of the magnetic field, for example, +90 deg for N-S direction and -90 deg for S-N direction.

- The involved MQ nodes may additionally have a helical arrangement along the closed loop

The above considerations are for permanent magnetic field. In case of alternative magnetic field, the commonly dependable synchronizations of the left and right-handed nodes are time dependable.

The EQ type node might be stationary (around charged particle) or running type, passing from one to another CL node. The EQ type node possesses larger energy than MQ type. **The photon wavetrain is a complex arrangement of running EQs with decreasing deformation gradient from the central axis of the wavetrain to its boundary radius, where running MQs are formed.** Thus, the photon wavetrain has boundary conditions (a solution of one long standing problem).

The analysis of the CL node dynamics as EQ and MQ type and the unveiled photon wavetrain structure in a normal CL space (possessing a normal Zero Point Energy) are presented in Chapter 2 of BSM thesis. CL space with subnormal Zero Point Energy is related to superconductivity effects. The CL node dynamics and the charge particles behaviour in this state of the matter-space complex is analysed in Chapter 4 of BSM.

The applied new approach allows also unveiling the real physical structures of the atomic and subatomic particles. The Bohr atomic model appears to be only a mathematical model providing correct energy levels, but it is not identical to the physical one. When taking into account the vacuum structure and the structure of elementary particles, the physical models of the Hydrogen and all stable elements appear quite different.

From a BSM point of view, the interpretation of the scattering experiments does not provide correct real dimensions, because the structures of the vacuum and elementary particles are not taken into account. BSM analysis found that the stable particles, such as proton, neutron and electron (and positron) posses structures with well defined spatial geometry and denser internal lattices. They are comprised of complex but understandable three-dimensional helical structures whose elementary building blocks are the same as those involved in the vacuum grid - the two types of prisms. Analysing the interactions between the vacuum space and elementary particles, but from a new point of view, the BSM theory allowed a derivation of number of

useful equations, such as a light velocity equation - expressed by the CL space parameters, a mass equation (the mass we are familiar with), an equation about the vacuum energy (zero point energy), and some relations between CL space parameters and the known physical constants. The BSM provides also an understandable physical explanation of what is an elementary electrical charge and why it is constant.

The motion analysis of the smallest charge particle - the electron from a new point of view (Chapter 3 and 4 of BSM) allows to unveil its physical structure and intrinsic properties. The electron is a system comprised of three helical structures as illustrated by Fig. 2. Two of its helical structures possess denser lattices located in the internal space of the helix envelopes (not shown in Fig. 2).
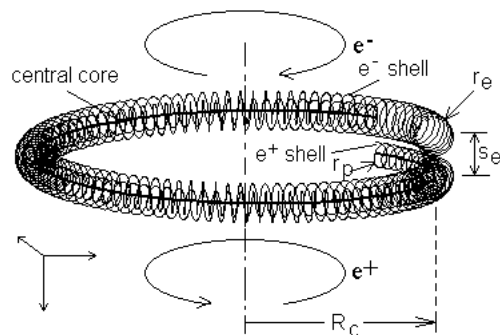

Fig. 2

Oscillating electron

External helical structure with internal denser lattice (from right handed prisms, for example) is referenced in BSM as external electron shell. It is responsible for the modulation of the CL space around the electron and creation of a negative charge. The internal helical structure with internal denser lattice (from a left-handed prisms, respectively) with a central core (from right handed prisms) is an internal positron. Regarded as a 3 body oscillating system the electron has two proper frequencies:

- first proper frequency: between the external electron shell and the internal positron
- second proper frequency: between the internal positive shell and the central negative core.

It is found that the first proper frequency of the electron is equal to the SPM frequency of the CL node. This is well known Compton frequency.

It is found that in conditions of screw-like motion of the electron with tangential velocity equal to the light velocity, the phase of the first

proper frequency of the rotating electron matches the phase of the SPM vector. They both oscillate with a Compton frequency. In the same time, the phase of the internal core (with a proper frequency of three times the Compton frequency) also matches the electron oscillations appearing as a third harmonic. Consequently, this is a motion condition with maximum interaction between the electron and CL space - a kind of quantum interaction. This type of motion is referred as an optimal confined motion of the electron. Its axial velocity is equal to $V_{ax} = \alpha c$. The corresponding electron energy is 13.6 eV. In such type of motion the helical step, s_e, is expressed by the following relations:

$$s_e = \frac{2\pi R_c \alpha}{\sqrt{1 - \alpha^2}} = \frac{\lambda_c \alpha}{\sqrt{1 - \alpha^2}} = 1.7706 \times 10^{-14} \ (m) \qquad [(3.9)]$$

$$s_e = g_e r_e = 2.002319 r_e \qquad\qquad [(3.12.a)]$$

where: R_c - is the Compton radius, α - is the fine structure constant, g_e - is the gyromagnetic factor, λ_c - is the Compton wavelength (CL space parameter).

From the analysis of the Fractional Quantum Hall experiments in Chapter 4 of BSM, it is found that: $r_p / r_e = 2/3$. Then all the of geometrical parameters of the electron are determined.

The configuration of one of the internal lattices of the helical structures of the electron called a Rectangular Lattice (RL) is shown in Fig. [2.16].
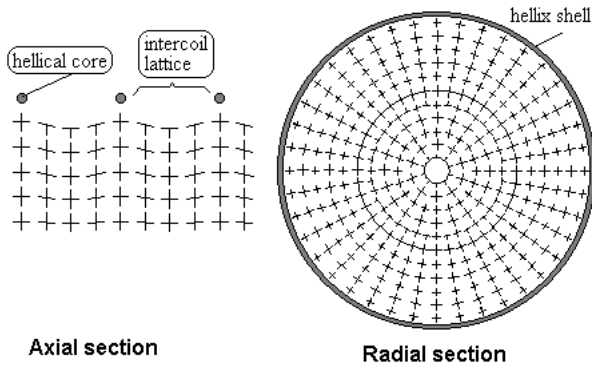

Fig. [2.16] Configuration of internal lattice of type RL (Rectangular Lattice) inside the cylindrical space enveloped by the first order helical structure

Every RL node is comprised of six prisms of the same type. The axial section contains number of concentric layers. The most external layer is IG connected to the helix, while every internal layer is connected to the neighbouring external one. The thickness of every internal layer is half of the thick-

ness of the neighbouring external layer. The stiffness of RL defined by the prism density is about 1000 times larger than the CL stiffness. Consequently, the volume of RL structure is not penetrative even for folded CL nodes. Then it displaces the CL structure, or in other words, it feels a CL pressure. This is a Static CL pressure discussed later. For open helical structures like those in the electron (the both ends are not connected) the internal RL structure is stabilised by twisting. In such way, it becomes a twisted type of RL structure, denoted as RL(T). The twisted radial stripes of RL(T) modulate the CL nodes converting them to EQ type nodes with proper spatial arrangement. This is the electrical field of the particle. The axial section of this in respect to the helical structure axis in close proximity to the particle is illustrated in Fig. [12.7].

In a far field, however, the E-filed lines, from the whole structure, appear as emerging from a point source.
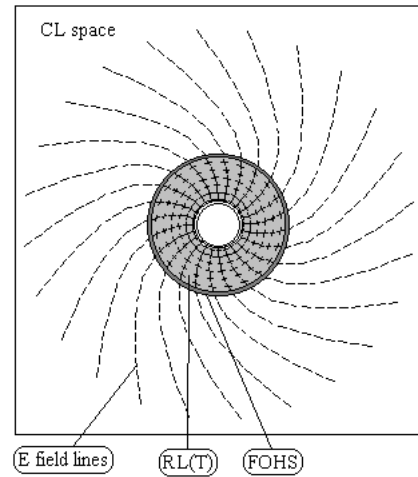

Fig. [2.17] Near E-field from RL(T) structure

The RL and RL(T) parameters are determined in Chapter 6 of BSM, where the physical meanings for number of experimental data from the particle physics are unveiled, such as: the ratio between pion-muon mass, the tau particle (Regge resonance at 1.7778 MeV), the resonance at 1.44 MeV, the Fermi coupling constant G_F, the effective mixing parameter $\sin^2\theta_{eff}^{lept}$, the energy equivalence of the "masses" of the W+- and Z bosons.

By using the unveiled structure of the electron as a reference etalon, the basic parameters of the CL space are obtained and expressed by the

known physical constants. The basic parameters are: the Static CL pressure - related to the Newtonian mass, the Dynamic CL pressure - related to the Zero point Energy of vacuum, the Partial CL pressure - related to the inertial properties of the atomic matter in CL space, the Compton frequency as a characteristic parameter of CL node and electron oscillating properties, the light velocity and the Compton wavelength. The obtained expression of Static CL pressure is:

$$P_S = \frac{m_e c^2}{V_e} = \frac{h v_c^4 g_e^2 (1 - \alpha^2)}{\pi \alpha^2 c^3} \quad \left[\frac{N}{m^2}\right] \qquad (3.53)$$

The static CL pressure allows defining the Newtonian mass (the mass we are familiar with) for any particle in a stable phase.

$$m = \frac{P_S}{c^2} V_H \qquad\qquad [(3.48)]$$

where: V_e is the envelope volume of the electron and V_H - is the total volume of similar structures for a particle under consideration.

The energy from displaced CL nodes can be directly estimated by the known equation $E = mc^2$.

When the electron or any stable helical structure is in motion it only displays the CL nodes. They are temporally folded, then displaced and again returned and unfolded to their initial positions. This is the inertial interaction that any moving helical structure exhibits in CL space. Consequently, displaced nodes exist permanently around the atomic particles in motion in respect to the CL space. The amount of the displaced nodes could be expressed by a CL space parameter Partial CL pressure. In Chapter 10 of BSM, it is found that the ratio between Partial and Static CL pressure is related to the fine structure constant by the relation:

$$P_P/P_S = \alpha^2/\sqrt{1 - \alpha^2} \qquad\qquad (10.18)$$

The confined screw like motion of the oscillating electron in CL space is characterized by strong quantum interactions with the oscillating CL nodes. This effect is contributed by two conditions: a phase match between the involved cycles (discussed above) and conditions of integer number of Compton wavelengths for boundary conditions of the induced magnetic field from the rotating electron. These two conditions allow strong quantum

effects to appear at particular velocities of screw-like motion of the electron, corresponding to the energy levels of 13.6 eV, 3.4 eV, 1.51 eV, 0.85 eV and so on.

The magnetic radius r_{mb} in a plane normal to V_{ax} is defined from the conditions that the rotating IG field of the internal lattice of the electron helical structure (that modulates the CL space) could not exceed the light velocity.

The magnetic radius for 13.6 eV is verified from the analysis of the quantum magnetic field (see §3.11 in Chapter 3 of BSM thesis): $\Phi_0 = h/q_o$ The accurate value of r_{mb} for 13.6 eV is almost equal to R_c, but slightly larger due to a finite thickness of the electron helical structure.

If relating the above energy levels with the number of full rotations of the electron one obtains:

13.6 eV - 1 rotation per SPM cycle
3.4 eV - 1/2 rotations per SPM cycle
1.51 eV - 1/3 rotations per SPM cycle
0.85 eV = 1/4 rotations per SPM cycle
1 SPM cycle = Compton time

BSM uses a parameter called **subharmonic number** in order to notify the quantum motion conditions of the electron. A motion with a first harmonic velocity corresponds to 13.6 eV, with a second subharmonic - 3.4 eV, with a third subharmonic - 1.51 eV and so on. The introduced parameter subharmonic number defines the spin motion behaviour of the electron in a classical sense.

Investigating the efficiency of the quantum interactions between the confined moving electron and CL space at relativistic velocities the relativistic gamma factor is derived in §3.11.A. The analysis provides a physical explanation of the relativistic effect of mass increase. It is a result of the finite rate at which the CL node could be folded and displaced. A limiting factor of this rate is the resonance frequency of CL node, estimated in §2.11.3, Chapter 2 of BSM, as:

$$v_R = 1.092646 \times 10^{29} \ (Hz) \qquad\qquad (2.55)$$

3. Quantum loops and possible orbits for electron with optimal confined velocity. Embedded signature of the fine structure constant.

3.1 Quantum motion of the electron

The motion of the electron is always a result of external forces, so its preferred motion is always

a screw-like. From the other hand, its simultaneous oscillations interact with the oscillating nodes. Let considering a repetitive motion in a closed loop. Obviously, the length of such loop will depend of the conditions of phase matching between the SPM frequency of the CL node, from one side and the first and second proper frequencies of the electron, from the other. All of them can be expressed by the Compton frequency.

Let us find the path length at which the quantum loop condition for the electron system is fulfilled. It is reasonable to look for path length defined by some CL space parameter. One of this parameter is the Compton wavelength $\lambda_c = \lambda_{SPM}$ If an electron possessing a first harmonic velocity travels in a closed loop with length λ_c, the number of turns N_T is:

$$N_T = \lambda_c / s_e = 137.03234 \qquad [(3.43.d)]$$

The value of N_T could be regarded as a condition of spin motion at which the initial phase in any one point of the closed loop is repeated. It is slightly different from the reciprocal value of the fine structure constant.

$$1/\alpha = 137.03598949$$

Therefore, the round number of turns is:

$$\overline{N_T} \approx 1/\alpha \qquad [(3.43.e)]$$

The obtained number of turns as $1/\alpha$, however, is not a whole number. In the same time, the trace length of this loop is quite small, when comparing to the proton dimensions (determined in Chapter 6). Therefore, we may look for the phase conditions at larger loop length. The close value of N_T to $1/\alpha$ is not occasional. Then, one may substitute the N_T with $1/\alpha$ and multiply the result by λ_c that is associated with the circumference length of the electron coil. Then we obtain:

$$N_T \lambda_c \approx \frac{1}{\alpha} \lambda_c = 3.249187 \times 10^{-10} \quad (m) \qquad [(3.43.f)]$$

We see that the obtained value with dimension of length is equal to the Bohr orbit length:

$$2\pi a_o = 3.3249187 \times 10^{-10} \quad (m) \qquad [(3.43.g)]$$

where: $a_o = 0.52917725 \times 10^{-10}$ (m) - is the radius of the Bohr atomic model of hydrogen.

We obtain one amazing result: the obtained loop length is equal to the orbit length of the Bohr atom. The orbit length defined by Bohr atomic radius is very basic parameter in the Quantum mechanics. From a point of view of BSM however, the physical meaning of this parameter is different.

According to BSM concept, the well known parameter a_0 used as a radius in the Bohr model, appears to be defined only by the quantum motion conditions of the electron moving in a closed loop. Then the main characteristic parameter of the quantum loop is not its shape, but its length.

For optimal confined velocity the number of electron turns in the quantum orbit is equal to the orbital length divided by the helical step (s_e).

$$\frac{2\pi a_o}{s_e} = \frac{\lambda_c}{\alpha s_e} = 18778.362 \qquad [(3.43.h)]$$

Substituting s_e in Eq. [(3.43.h)] with its value from Eq. (3.9) we get:

$$\frac{2\pi a_o}{s_e} = \frac{\lambda_c}{\alpha s_e} = \frac{\sqrt{1-\alpha^2}}{\alpha^2} \qquad (A)$$

Consequently, we arrive to the conclusion:

(A) The number of full turns of the electron in a quantum loop is defined only by the fine structure constant.

We must not forget that the condition (A) is possible due to the dynamical interactions between the oscillating electron and the oscillating CL nodes. The analysis of the confined motion of the electron in Chapter 3 and 4 of BSM indicates that its second proper frequency is three times higher than the first one. Then the accurate value for the fine structure constant could be estimated by investigating the following probable options:

Option (1): the phase repetition is satisfied only for the secondary proper frequency:

Option (2): the phase repetition is satisfied for both the first and secondary proper frequency.

In option (1), the value of 18778.362 should be replaced by 18778.33(3) in which case the central core of the electron will make a whole number of cycle: $3 \times 18778.33(3)) = 56335$ full cycles. Combining Eq. [3.43.h)] with Eq. [(3.9)], we get:

$$\sqrt{1-\alpha^2} = 18778.33(3)\alpha^2$$

Solving for alpha we obtain: $\alpha = 7.2973587 \times 10^{-3}$, but this is only a probable option.

In option (2), we may search for the lower value of the number of the electron rotations in the

quantum loop. According to the conclusion (A), we may check initially by some number determined by the fine structure constant. In the same time, this number should be larger than one, so the only possibility is the reciprocal value of the fine structure constant. Multiplying Eq. (A) by $1/\alpha$ one get:

$$\frac{2\pi a_o}{s_e} = \frac{\sqrt{1-\alpha^2}}{\alpha^3} = Integer \quad\quad\quad (B)$$

The Eq. B may provide criterion for obtaining the most accurate value of alpha only if the experimentally determined value exceeds some accuracy threshold. From the other side, the analysis leads to a guessed conclusion that the number $1/\alpha \approx 137$ (approximately 137 orbital cycles) may define the lifetime condition for the electron in a particular orbit (corresponding in the present case to a first harmonic electron velocity whose kinetic energy is 13.6 eV), corresponding to an exited state of the orbiting electron in the atom. This lifetime should be valid for the spontaneous emission. The CL space could be pumped, however, for much less number of orbit cycles. This is reasonable, because the pump energy from the oscillations with secondary proper frequency (central core oscillations) is much smaller that the pump energy from the oscillations with the first proper (Compton) frequency. Such consideration is in agreement with the effect of stimulated emission.

The provided analysis leads to a conclusion that a closed loop orbit with trace length of $2\pi a_0$ is a characteristic feature of the quantum behaviour of the orbiting electron in the case when its axial velocity corresponds to the first harmonic number (energy of 13.6 eV).

The quantum motion parameters of the electron in a quantum loop for velocities corresponding to different subharmonic numbers are shown in Table 1.

Table 1

No	E (eV)	V_{ax}	V_t	r_{mb}	l_{ql}	L_q (A)
1	13.6	αc	c	$\sim R_c$	$2\pi a_0$	1.3626
2	3.4	$\alpha c/2$	$c/2$	$2R_c$	$2\pi a_0/2$	0.6813
3	1.51	$\alpha c/3$	$c/3$	$3R_c$	$2\pi a_0/3$	0.4542
4	0.85	$\alpha c/4$	$c/4$	$4R_c$	$2\pi a_0/4$	0.3406
5	0.544	$\alpha c/5$	$c/5$	$5R_c$	$2\pi a_0/5$	0.2725

where: E - is the electron energy, V_{ax} - is the axial velocity, V_t - is the tangential velocity of the rotating electron structure, r_{mb} - is the value of the boundary electron magnetic radius in a plane normal to V_{ax} vector, c - is a light velocity, R_c - is the Compton radius, a_o - is the Bohr radius, l_{ql} - is the trace length for a motion in closed loop (single quantum loop), L_q - is the length size of the quantum loop as Hippoped curve with parameter $a = \sqrt{3}$.

The introduced parameter **subharmonic number** shows the rotational rate of the whole electron structure. The rotational rate decreases with the consecutive increase of this number. From the provided analysis we find that the electron makes 18778.362 rotations for one quantum loop. One quantum orbit may contain one ore more quantum loops. From Table 1 we see that for a confined moving electron the circumference length of the boundary of the electron's magnetic radius in a plane normal to V_{ax} is equal to a whole number of λ_c. The Compton wavelength, λ_c, is a characteristic parameter of CL space. It is an attribute of Zero Point Waves existing in CL space, that from their side and related to the known physical parameter **permeability of the free space.**

3.2. Quantum orbits. Emission and absorption of photon.

It is apparent from the provided analysis that a stable quantum loop is defined by the repeatable motion of oscillating electron. The shape of such loop is defined by external conditions. Such conditions exist in the following simple cases:

- a quantum loop obtained between particle with equal but opposite charges and same mass, as in the case of positronium (see Chapter 3 of BSM)

- a quantum loop obtained between opposite charges but different masses, as in case of the hydrogen atom.

In both cases we may call these loops **quantum orbits**. In case of hydrogen, the quantum loop should possess fixed symmetry in respect to the proton.

The unveiled intrinsic conditions of the quantum loop allow definition of possible quantum orbits in atoms and molecules. The most simplest examples are the possible quantum orbits of hydro-

gen atom. In Chapter 7 of BSM a model of Balmer series is suggested. Its analysis confirms the concept of confined motion of the electron. The trace length of the quantum orbit of Balmer series match the quantum loop No 2 from Table 1. The same quantum loop exists also in Deuteron. The BSM model of Hydrogen is different from the Bohr model, but all types of quantum numbers are identifiable. The quantum levels are obtainable by considering a whole number of Compton wavelengths but in a specific conditions defined by factors, such as the proximity distributed E-field of the proton, and its Intrinsic Gravitation field.

It appears that the limiting orbit has a length of $2\pi a_0$ and all other quantum orbits are inferior. This is valid not only for Balmer series in Hydrogen but also for all possible quantum orbits in different atoms, if they are able to provide line spectra. Therefore, the suggested physical model provides **a solution of the boundary conditions problem of the electron orbits for the Hydrogen and for all other atomic models suggested by BSM theory.**

The analysis of interactions between the oscillating electron in confined motion and oscillating CL nodes allows unveiling the process of the photon generation. According to the BSM concept, the emission of a photon, contributing to line spectra, is a result of **pumping of CL nodes** from the orbiting and simultaneously rotating and oscillating electron. In this process more than one orbital cycles are involved. **The emission of a photon occurs from the surrounding CL space in the moment when the electron drops from higher to lower energy orbit. This explains why the Quantum mechanical model needs an uncertainty principle, while the BSM model does not need such.**

In the Quantum Mechanical model the CL substance is missing and the process of the photon generation has to be directly connected to the orbiting electron. In such case, it seems that the electron position could not be located, so a concept of "electron cloud" has been introduced. In BSM model the electron in the atom has well defined orbit, while the concept of CL space allow analysis of the electron motion in any portion of the orbit.
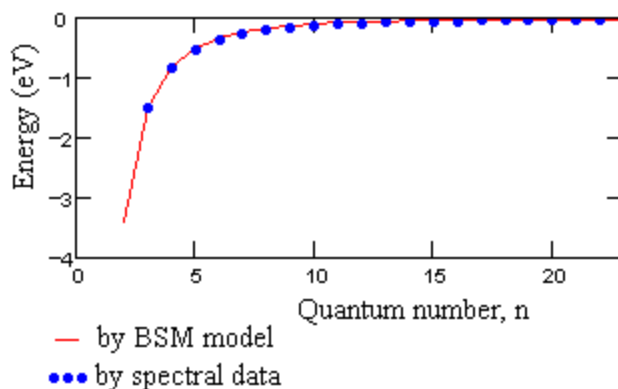

Fig. [7.19] Comparison between calculated and experimental energy levels for Balmer series

Fig. [7.19] illustrates the close match between the energy levels calculated by BSM model of Balmer series in Hydrogen and those provided by the Quantum mechanics.

The electron with unveiled structural parameters is used also as a probe for estimation of the CL space parameters and formulation of mass equation valid for Newtonian mass (the mass we are familiar with). The Newtonian gravitation (the universal gravitational law we are familiar with) appears as a special case of IG law in CL space, and it is valid only between atomic matter structures.

4. External shape and geometry of proton and neutron

It is known from the particle physics experiments that the electron (positron) is an end product in the most frequent reactions of the type: pion - muon - electron (positron) or charged kaon - pion - muon - electron (positron). This feature allows using the unveiled structural and interaction parameters of the electron in order to solve the inverse task: to restore and find the physical structures of muon, pion, kaon and finally the structure of the stable particles proton and neutron. For this purpose, the derived mass equation Eq. [(3.48)] and its modification are used in the analysis provided in Chapter 6 of BSM. When applied for the proton, the parameter V_H takes into account the total volume of all helical structures defined by the volume of their internal Rectangular Lattice. The unknown parameters of mass budget are obtained by using accurately measured experimental data from particle physics but applied according to their corre-

spondence to the unveiled physical models, according to BSM. One still missing parameter for solution of the necessary set of equations is the length of the proton central core (L_{PC}). It, however, participates in the proton envelope that is found out to be involved in a permanent interaction process with a Zero Point Waves of CL space. It is found that these waves, permanently persistent in CL space, are directly related to the background temperature of CL space. A theoretical expression of this temperature is derived in Chapter 5 of BSM by using the concept of Zero Point Waves (ZPW) bouncing on the envelope surface of the proton. In conditions of dynamical equilibrium, the energy of the bouncing ZPW is equal to the energy radiated from the atoms and molecules, dispersed in the interstellar space. The signature of this process according to BSM concept is the measured Cosmic Microwave Background (CMB) corresponding to temperature of 2.72 K. In the derivation of the theoretical equation of this temperature the following physical laws and parameters are involved: the ideal gas law, the Avogadro number, the proton geometrical parameters, the relation between the magnetic moments of electron and neutron (neutron is used more accurately instead of proton in order to reflect the neutrality of the involved atoms and molecules contributing to the CMB).

$$T = \frac{N_A^2}{S_W} \frac{h \nu_c (R_c + r_p)^3 L_{pc}^2}{2 c R_c r_e R_{ig}} \left(\frac{\mu_e}{\mu_n}\right) = 2.6758 \text{ K} \qquad [(5.8)]$$

where: $S_W = 1 \ m^2$ participates as a reference surface in SI system, μ_e and μ_n - are the magnetic moments of electron and neutron, respectively.

The approximate determination of the L_{PC} from Eq. [(5.8)] allows to solve a set of mass budget equations in Chapter 6 of BSM. In these equations, some additional data are used from the particle physics, such as: the mass of eta particle, the antiproton/proton ratio of stopping power, and the energy-mass equivalence of W bosons and tau particle. The calculations allow accurate determination of the proton (neutron) geometrical parameters and its internal structure. The proton is a twisted torus with a curled shaped external helical structure of positive prisms. Inside this envelope there are two pions (positive and negative) also with shape of curled twisted toruses but with larger secondary helical step. One central kaon structure

has a similar shape as the envelope of the twisted proton. When broken in one place the external helical structure envelope of the proton (neutron) is completely destroyable. The measured masses of the broken in one place pions and kaons exhibit extremely small standard deviations. In an open loop configuration, however, these particles are not stable, so they decay. More often, the kaon decay into pions, and the pions decay into muon, whose shape is like a multiturn electron (or positron) structure. Then the decay of muon is accompanied by destruction of its internal Rectangular Lattice (also twisted) that is much denser than the Cosmic Lattice. During this process an enormous energy is released. This energy gives the infinities in the Feynman diagrams. Some signatures of released energies from RL destruction of helical structures, for example, are the following: the experimentally estimated energies corresponding to the "mass" of W^- and W^+ bosons (from the kaon structures, according to BSM); the experimentally measured energies corresponding to the "mass" of the tau particle and the Regge resonance at 1.44 GeV (both from the helical structures of the normal electron, according to BSM). All high order helical structures are built of same lower order helical structures similar as the single turn structure of electron (with internal lattice) but they are multiturn, instead. The parameters r_e and r_p of all type helical structures, however, are almost unchangeable.

The proton core length (L_{PC}) is cross-validated by the Balmer series model (Chapter 7 of BSM) and by vibrational models of some simple molecules (Chapter 9 of BSM).

The proton is a twisted torus with a shape close to a figure 8, while the neutron is a same structure but in shape of double folded torus. More accurately the plane projection of the proton envelope is quite close to a Hippoped curve with parameter $a = \sqrt{3}$. The twisting (and folding) direction is strongly defined by the underlined structures of pions and kaon inside the proton (neutron) envelope. Consequently all protons (and neutrons) involved in atomic nuclei have one and a same

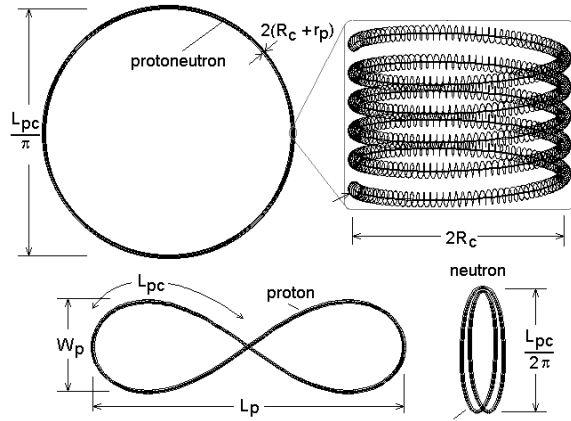handedness. The shapes of the proton and neutron are shown in Fig. 3.

Fig. 3. Geometrical parameters of the proton and neutron. The magnified view shows only the external helical shell without the internal structures of pions and kaon (extraction from Atlas of ANS)

The estimated geometrical parameters of the proton (neutron) are given in Table 2. The calculated physical dimensions of proton and neutron appear quite different from those obtained by the scattering experiment. However, important factors such as the vacuum grid and the particle structures are both not taken into account in the interpretation of these experiments.

The proton and neutron both have exactly the same internal structure but they are distinguishable by their overall shape (and a slight difference in their internal structural twisting that provides a slight mass difference).

Table 2

Parameter	Value	Description	Calculations and cross validations in:
L_{PC}	1.6277 (A)	proton (neutron) core length	Chapters 5 and 6
L_P	0.667 (A)	proton length	Chapters 6, 7, 8, 9
W_P	0.19253 (A)	proton (neutron) width	Chapters 6, 7 ,8 ,9
r_e	8.8428E-15 (m)	small radius of electron	Chapters 3, 4, 6
s_e	1.7706E-14 (m)	electron(positron) step	Chapter 3
r_p	5.8952E-15 (m)	small radius of positron	Chapters 3, 4, 6
$2(R_c + r_p)$	7.8411E-13 (m)	thickness of proton (neutron)	Chapters 6, 7, 8, 9

Then a question may arise: why the proton possesses a charge while, the neutron - not. The answer is: The electrical charge is a result of the modulation of CL nodes by the RL(T) lattice of the helical structures (external shells). In case of neutron, all helical structures get overall symmetry in respect to its axis. In this shape the modulation of CL space in the far field is compensated and the electrical field is a zero. In case of proton, the overall torus is twisted and the axial symmetry of RL(T) is destroyed. Therefore, it is able to modulate the CL node in the near and far field.

In fact the modulation symmetry for the neutron is not perfect in the near field as in the far field,

so the neutron still exhibits some modulation of the CL nodes and consequently an electrical field, but only in a proximity range. This field is locked by the stronger IG field in the proximity range to its envelope so it is not detectable in the far field. The locking mechanism of IG field, although, does not work well when the neutron is in confined motion in CL space, so it exhibits a magnetic moment (the magnetic moment of the neutron as a neutral particle has not been satisfactorily explained so far). The electrical field of the proton is always unlocked due to its different overall shape. Therefore, in the far range the electrical field of the proton appears as emerging from a point, but in the

near field, it is distributed over the proton's envelop. In Chapter 2 of BSM, it is shown that the EQ node has a larger oscillating energy than the MQ node. Then the electrical charge regarded as a system of EQs possesses some energy. From this point of view the energy of the electrical charge appears as a part of the total energy balance involving the Intrinsic Gravitation and the zero Point Energy of the vacuum. In this total balance, the IG field manage the energy portion of electrical field in a way that the unity charge of any single charge particle appears as a constant.

Fig 3 shows the spatial geometry of the Deuteron, where: *p* - is the proton and *n* - is the neutron. The neutron is centred over the proton saddle and kept by the Intrinsic Gravitation (IG) field and the proximity electrical fields of the neutron and proton. In such conditions the neutron is kept stable (it is not able to unfold and convert to proton).

Fig. 4 illustrates the protons and neutrons arrangement in the nucleus of He. In such close distance, the internal lattices of the proton's helical structures are kept by IG forces that are inverse proportional to the cube of the distance. The nucleus of helium is the most compact atomic structure. Therefore, its influence on the CL space parameters is the strongest one. As a result, the helium nucleus possesses the largest binding energy between the involved protons and neutrons.
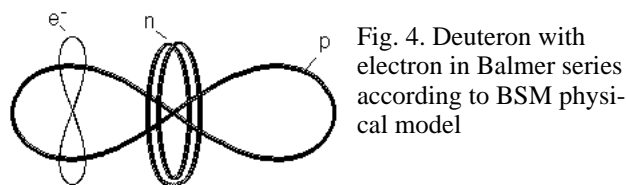

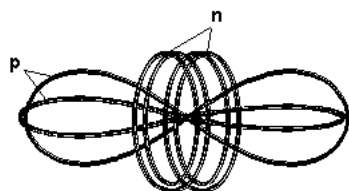Fig. 4. Deuteron with electron in Balmer series according to BSM physical model

Fig. 5. Helium nucleus according to BSM physical model

When taking into account the two features of the proton: a finite geometrical size and the distributed proximity electrical field it is evident that the Coulomb law is valid down to some limit, defined by the finite size of the proton structure. This is verified by the model of Balmer series in Hydrogen

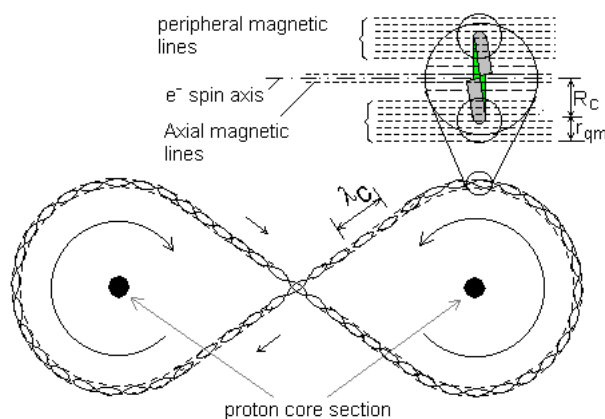presented in Chapter 7. The idealized shape of Balmer series orbit is shown in Fig. [7.7].

Fig. [7.7]. Idealized shape of Balmer series orbit. R_c - is the Compton radius, r_{qm} - is a magnetic radius of electron at sub optimal quantum velocity. The Compton wavelength λ_c shown as standing waves is is not in scale

5. Atlas of Atomic Nuclear Structures

5.1. Physical atomic models according to BSM concept.

One of the most useful results of BSM theory with practical importance is the Atlas of Atomic Nuclear Structures (ANS). The analysis leading to unveiling the spatial arrangement of the protons and neutrons in atomic nuclei is provided in Chapter 8 of BSM. It shows that the protons and neutrons follow a strict spatial order with well defined building tendency related to the Z number of the elements. The signature of this tendency matches quite well the row-column pattern of the Periodic table, the Hund's rules and the Pauli exclusion principle. The Atlas of ANS provides nuclear configurations of the elements from Hydrogen to Lawrencium (Z = 103). For drawing simplification of the nuclear structures, the protons and neutrons are presented by simplified patterns reminding their shape. The left part of Fig. 6 shows the patterns used for the proton, deuteron, tritii and helium,
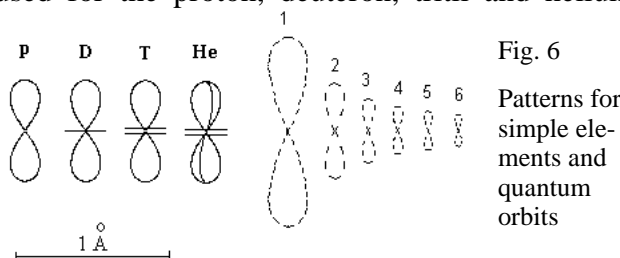

Fig. 6

Patterns for simple elements and quantum orbits

while the right part shows the most common shapes and possible dimension of the quantum orbits. The dimensions of the quantum orbits and the proton and neutron are given in one and a same scale.

In the Atlas of ANS, the pattern of proton is symbolized by arrow in order to simplify the drawings. Additional symbols are also used for the same reason.

For any atomic nucleus, a polar axis can be identified. It is defined by the long symmetrical axis of one or more He nuclei in the middle of atomic nucleus. The atomic nuclei posses also twisting features due to the proton twisting, but it is not shown in the drawings. In the Atlas of ANS additional symbolic notations are used for the unveiled types of proton's bonds and pairing in which IG and EM fields are involved.

5.2. Three-dimensional structure of atomic nuclei and limited angular freedom of the valence protons.

The Atlas of Atomic Nuclear Structures provides the nuclear configurations of the stable isotopes. One or more He nuclei are in the nuclear centre, aligned with the polar axis of symmetry. The peripheral building blocks of the lighter elements are usually deuterons, while the element tritii appears more frequently in the nuclei of heavier elements. The positions of the protons are defined by the consecutive number of proton's shell and by the type of the bonds between the protons.
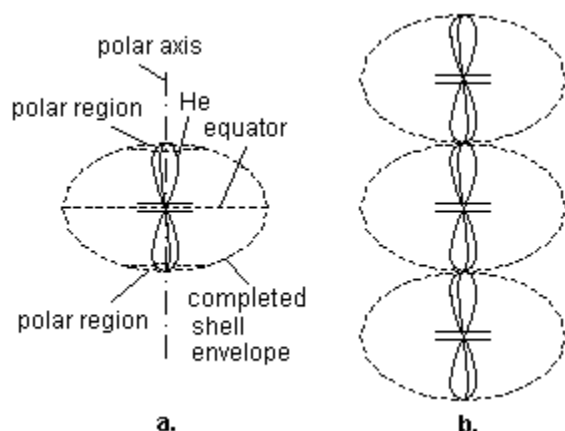
and neutrons, having in mind the repulsive forces from the proximity fields of the protons. The polar chain structure appears for the atoms with Z > 18 (after Argon).

The structural restrictions of the positions of the atoms in the molecules comes from two factors:
   - stable structural arrangements of the bonded protons of the nucleus
   - angular restrictions of the valence protons.
   The following type of bonds are unveiled.

Bonds in the atomic nuclear structure   *Table 8.1*

===

Bond notation	Description
GB	Gravitational bond by IG forces
GBpa	polar attached GB
GBpc	polar clamped GB
GBclp	(proton) club proximity GB
GBnp	neutron to proton GB
EB	electronic bond (weak bond)

The gravitational bonds are held by the IG field of the intrinsic matter (more explicitly the IG field of the internal lattices of the helical structures from which the proton and neutron are built). The IG field controls also the proximity E-field of the proton (and proximity locked E-field of neutron) and its unity charge appearance. For this reason, all GB types of bonds are very stable.

The four types of the gravitational bonds and one type of electronic bond are illustrated in Fig. [8.4], where the positions of some quantum orbits are also shown.
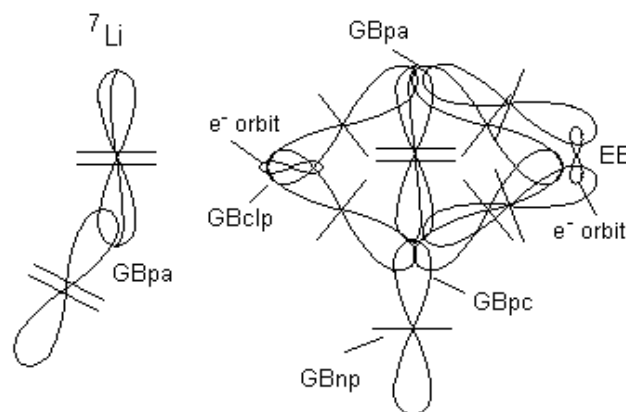

Fig. [8.2]

a. - polar structure; b. - polar-chain structure

Fig. [8.4]

The left-side structure is ^{7}Li nucleus,. The right-side structure is only a portion of nucleus showing the different type of bonds, according to Table [8.1]. The planes of the shown quantum orbits in fact are normal to the drawing plane

Fig [8.2] illustrates the backbone structure of nucleus allowing the most dens pack of the protons

The GBpa and GBclp bonds can not have any freedom of motion. The GBpa bonds for valence protons have an angular restricted freedom of motion in a plane close to the polar section. The EB type of bonds are valid only for the valence protons but they are provided by electron orbit pairing, corresponding to the Hund rules. There are few types of such pairings. The two of them are more important: a first type - two orbits in separated parallel orbital planes; a second type - two electrons with different QM spins, according to a Pauli exclusion principle (their circling directions are opposite each other). The second type of Hund rule appears valid for EB bonds.

The GB type bonds could not be broken in any type of chemical reaction, but only in nuclear reactions where quite large energies are involved. The EB type of bond however is weak. Bonds of such type begin from the raw 13 of the Periodic table while in raw 18 (noble gazes) they are converted to GBclp bonds. The EB bonds normally exclude the external shell protons from chemical valence, so they play a role for the principal valence of the elements from group 13 to 17. This is valid for rows 1, 2, 3 of the Periodical table. In some conditions, however, the EB bonds could be broken, so the element may exhibit multiple oxidation numbers.

For some chemical compounds between elements with large number of valence protons, not all free valence protons can be connected by electronic bonds. This is a result of the finite nuclear size of the atoms and the angular restriction of the valence protons.

It is evident from the nuclear structure that the positions of the electron orbits are strictly determined by the positions of the protons with their proximity electrical fields and the conditions of quantum orbits provided by Table 1. **Therefore, the electron orbits are not shown in the Atlas of ANS but their positions are easily identifiable. Having in mind the above consideration the well defined orbital positions are characterized by the same first ionization potential embedded in the Quantum mechanical models and obtained experimentally.**

6. Electronic bonds between atoms in molecules

It is evident that the BSM model of the atom allows identification of the orbital planes and chemical bond orientation of the atoms in the chemical compounds. Additionally the quantum mechanical spin of the electron circling in orbit around the proton is also identifiable. The proton envelope is twisted torus, so it possesses a well-defined handedness along any one of its axes of symmetry. Then, the electron in the quantum orbit shown in Fig. 4 has an option to circle in two different direction in respect to the proton direction of twisting. This will corresponds to two slightly different energy levels. **Its signature is a fine structure splitting of the spectral line.**

The intrinsic conditions of the quantum orbits defined by the two proper frequencies of the electron and CL node dynamics are valid also for the bonding electrons in molecules. Let consider a most simple case of H_2 molecule identified as an ortho-I state. Its shape is illustrated in Fig. [(19.2)] In this figure the three-dimensional shape of the proton is replaced, for simplicity, by a 2-dimensional Hippoped curve with parameter $a = \sqrt{3}$. The molecular vibration in such simple system is of linear type. The long axes of the protons and quantum orbit are aligned with the molecular vibrational axis.
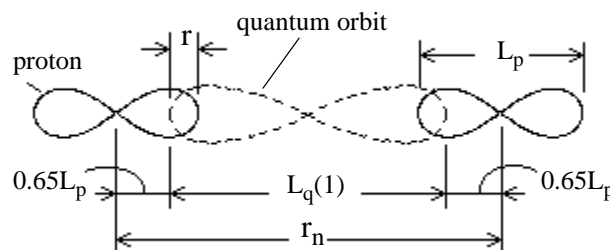

Fig. [9.12]
Structure of H_2 - ortho-I state molecule
L_p - is a proton length
$L_q(1)$ is a long side of a first harmonic quantum orbit
r_n - is the distance between the Hydrogen atoms
r - distance between the electron and the proton's core in the circular section (for the most external orbit
Note: The quantum orbit quasiplane is perpendicular to the quasiplane of the protons. However, they both are shown in one plane for simplification of the drawing

The both electrons circle in a common quantum loop (orbit) but in opposite directions (opposite QM spins). The quantum orbit crosses the Hippoped curves of the protons in the locus points. We may assume that every orbiting electron is able to neutralize one charge, by interconnecting its E-filed lines to the proton E-field. Let considering the moment, when both electron are in the locus points of the Hippoped curves, representing the protons. Their velocity vectors in this case are perpendicular to the direction of the molecular vibration and do not contribute to the momentum energy of the system. Then, their moment interaction can be estimated by considering only two unit charges at distance r_n. Now, let assume that the left proton and the right electron are both missing. The system energy in this case is $q/4\pi\varepsilon_o r_n$ [eV]. The same considerations and results are valid also for the other symmetrical case. Adding the energies from the two symmetrical cases we get the full system energy.

$$E = \frac{2q}{4\pi\varepsilon_0[L_q(1) + 0.6455L_p)]} = 16.06 \text{ eV} \qquad [(9.4)]$$

where: the factor 0.6455 defines the distance of the locus from the central symmetrical point of the Hippoped curve with factor $a = \sqrt{3}$.

The photoelectron spectrum of H_2 molecule shows one well identifiable parameter, called a Vertical Ionization Potential (VIP), which is extensively used in the Quantum mechanical calculations. Its value is:

$$E_{VIP} = 15.967 \text{ eV}$$

We see that the calculated energy by Eq. [(9.40] matches the experimental value of VIP with a fractional error of 0.58%. This coincidence allows to unveil the vibrational properties of the atoms in the simple diatomic molecules.

Fig. [(9.15)] shows the vibrational diagram of H_2 - ortho-I state molecule and the relation between the optical and photoelectron spectrum. The numbering 1 to 3 and 0 is used by BSM in order to match the accepted by QM numbering of optical vibrational bands $(0-\upsilon")$ and $(1-\upsilon")$ .. The parameter Δ in Eq. (9.23) corresponds to the vibrational levels but referenced to the equilibrium internuclear distance (corresponding to the bottom of the vibrational curve).
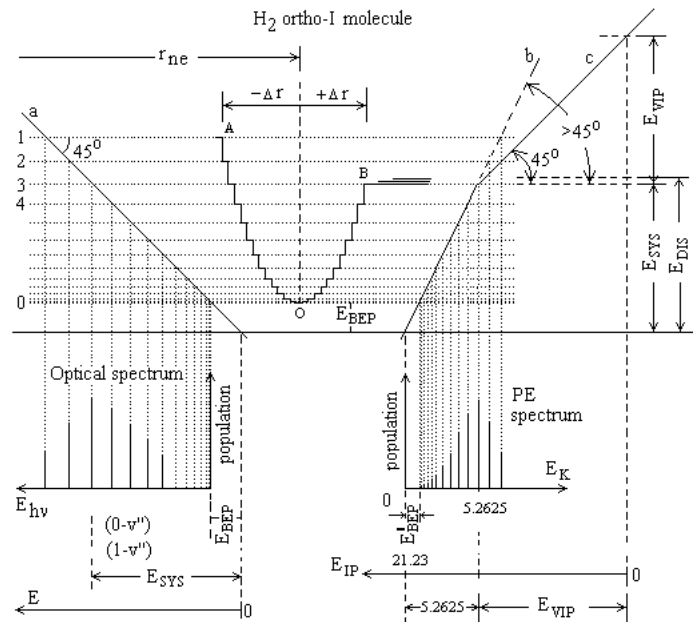

Fig. [9.15]
Vibrational diagram of H_2 ortho-I molecule
E - is a momentary energy scale
$E_{h\upsilon}$ - is a photon energy scale (not starting from zero)
$(0-\upsilon")$ and $(1-\upsilon")$ optical vibrational transition bands from Lyman system
r_{ne} - is an internuclear distance at equilibrium point
$-\Delta r$ and $+\Delta r$ are the ranges of displacement
E_{SYS} - is a system energy at point B, before dissociation
E_{DIS} - is a dissociation energy
E_{VIP} - is a Vertical Ionization Potential
E_{IP} - is a PE spectrum parameter (Ionization Potential)
E_K - is a PE spectrum parameter ("electron kinetic energy")
E_{BEP} - is a bound energy at equilibrium point
E'_{BEP} - is a "bound energy" estimated by PE spectrum

The analysis of the simple H_2 molecule allows to unveil the vibrational model of simple diatomic molecule in which the hidden so far Intrinsic Gravitation participates in the total energy balance of the system, including the energy embedded in the electrical charge of the participated electrons and protons. The parameter E_{BEP} is determined by cross-analysis of the optical and photoionization spectra. The obtained equation for the vibrational levels of H_2 ortho-I molecule based on a total intrinsic energy balance is:

$$E_V = \frac{C_{IG}}{q[[[L_q(1)](1 - \alpha^4\pi\Delta^2)] + 0.6455L_p]^2} - \frac{2E_q}{q} - \frac{2E_K}{q} \quad [9.23$$

where:

$$\Delta r = L_q(1)\alpha^4 \pi \Delta^2 \qquad\qquad [(9.26)]$$

$$C_{IG} = (2h\nu_c + h\nu_c\alpha^2 + E_{BEP}q)(L_q(1) + 0.6455)L_p) \quad [(9.17)]$$

$$C_{IG} = G_0 m_{n0}^2 = 5.26511 \times 10^{-33}$$

where: E_{BEP} [eV] - boundary energy at equilibrium point , h - Planck constant, ν_c - Compton frequency, α - fine structure constant, L_P - proton length (of the Hippoped curve), L_q - quantum orbit length as Hippoped curve (see Table 1), G_0 - intrinsic gravitational constant, m_{no} - intrinsic neutron mass (the proton have the same mass plus the mass-energy equivalence of the electrical charge it possessing), $E_q = h\nu_c$ - is the IG energy spent for creating the positive unit charge of the proton, E_K - is the kinetic energy of the electron, Δ - is a quantum vibrational number referenced to the equilibrium point (see Fig. [9.15])
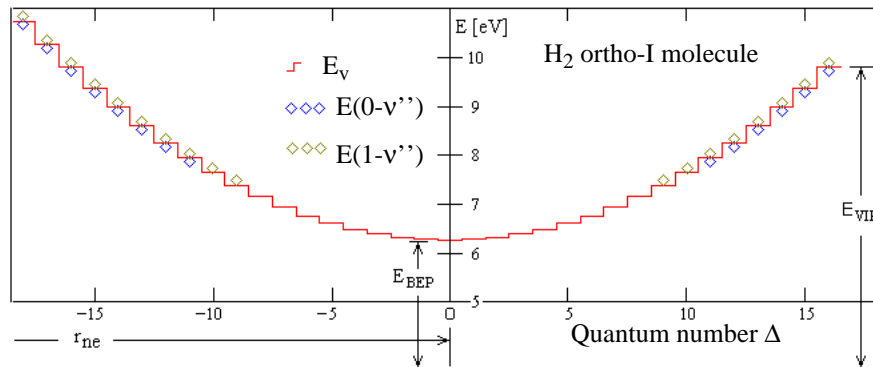
The term E_q/q takes into account the involvement of IG field of the proton for creating the positive proton's charge ($2E_q/q$ - for the two protons).

The parameter C_{IG}, called IG factor is involved in the cubic IG law and takes into account the amount of intrinsic matter involved in the proton (neutron). This parameter is cross-validated by calculation of the binding energy between the neutron and proton in Deuteron (Chapter 9 of BSM). The calculation is based on the estimation of the work for disintegration of Deuteron by moving the neutron from its initial central position along the long proton axis and using the inverse cubic IG law. The calculated in such way binding energy of 2.145E6 (eV) is pretty close to the experimentally measured binding energy of 2.222457 (eV). The IG factor is also validated by the comparison between the calculated vibrational levels by BSM models and the experimentally obtained spectra for some diatomic molecules (Chapter 9 of BSM).

Fig. [9.24] shows the energy levels E_v, calculated by Eq. [(9.23)] and vibrational levels of the optical transitions E(0-v'') and E(1-v''). The optical spectrum is from the system $(B \, {}^1\Sigma_u^+ - X \, {}^1\Sigma_g^+)$, known also as a Lyman system. Good experimental measurements of this system are provided by I. Dabrowsky (1984).

Fig. [9.24]. Energy levels E_v, calculated by Eq. (9.23) and vibrational levels of the optical transitions E(0-v'') and E(1-v''), corresponding to two QM spin values. The calculated levels are shown by step line, while the optical transitions by diamonds.

The fractional error between the calculated levels (E_v) by Eq. [(9.230)] and the optical data is within +/- 0.035%. The parameter $E_{BEP} = 6.2627$ eV is determined from the condition of minimum difference between the measured and calculated levels. It is used for accurate calculation of C_{IG} factor, used in Eq. [9.17].

Similar analysis is provided also for D_2 molecule since it is a more typical building element in the atomic nuclei. Following this type of analysis an analytical expression for vibrational levels for heavier and simple homonuclear diatomic molecules is obtained:

$$\Delta E(p, n, \Delta) = \frac{2\alpha C_{IG}(A - p)^2}{[r_n \pm [\Delta r(n, \Delta)]]^2} - pB_{D2}(n, \Delta) \qquad [(9.55)]$$

where: A - is the atomic mass for one atom in *daltons* (atomic mass units), p - is the number of protons involved in the bonding system (also per one atom), n - is the subharmonic quantum number

of the quantum orbit, r_n - is the internuclear distance at the equilibrium vibrational point.

It is found that the first harmonics quantum orbit $L_q(1)$ is possible only for H_2 and D_2 molecules. For diatomic molecules from heavier atoms the intrinsic balance is obtained only for larger subharmonics of the rotating and oscillating electron (corresponding to lower quantum velocities of the electron), or $L_q(2), L_q(3), L_q(4)$ and so on. Based on derived Eq. [9.23] and the data from optical and photoionization spectra the possible configurations of simple diatomic molecules are identified.

The conditions defining the intermolecular quantum orbits are different from those of atomic quantum orbits. For atomic orbits, the orbital defining conditions are referenced to the nucleus and not influenced by another nucleus. For intermolecular quantum orbits, however, the defining conditions are influenced by the nuclear motion of involved atoms, in which the IG field interactions are involved. The IG forces are able to modulate the spatial configuration of the proximity E-field of the protons involved in the chemical bond. As a result, the vibrational quantum conditions occur at intrinsically small changes of the internuclear distance (see Chapter 9). For H_2 ortho-I molecule, for example, the vibrational range is only 4E-16 (m) while the internuclear distance is 2.23E-10 (m). This effect in fact facilitates the method for unveiling of the possible configuration of any molecule, because it allows to use the estimated dimensions of $L_q(n)$. From the energy point of view $L_q(n)$ are valid for the limit orbits. Consequently: **The intrinsically small change of the internuclear distance allows applying the estimated dimensions of the limit orbits $L_q(n)$ in a drawing method for unveiling the internuclear distances.**

7. Method for determination the molecular structures of diatomic molecules

The molecular structures for diatomic molecules can be unveiled by using simultaneously the following methods:

- a drawing method using the nuclear structural considerations and angular restrictions of the electronic bonds with common scale dimensions of the basic building components and the possible quantum orbit

- a theoretical calculation of the vibrational level and corresponding internuclear distance by Eq. [(9.55)]

- matching the calculated data with identified spectral bands from the optical and photoelectron spectra.

Fig. [9.42] shows the photoelectron spectra of O_2 molecule. They correspond to different internuclear distances.
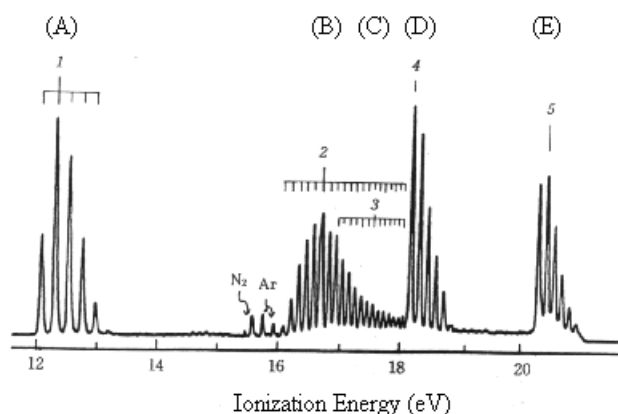

Fig. [9.42]. PE spectrum of oxygen molecule excited by He I radiation (Turner et all., courtesy of K. Kimura et al., (1981)). The capital letters in brackets is a notation used by BSM.

Table 9.6 shows the calculated internuclear distances for different quantum orbits L_q, using Eq. [(9.55)] and the estimated distances by the drawing method.

Table 9.6 shows the possible states of O_2 molecule obtained by the two methods and their possible correspondence to the states of the photoionization spectrum shown in Fig. [9.42].

Calculated by Eq. (9.55) values for r_n for **Table 9.6** O_2 states. The values are given in Angstroms (A).

r_n (A)	$L_q(2)$ (1 bond)	$L_q(2)$ (2 bonds)	$L_q(2x)$ (2 bonds)	$L_q(3)$ (2 bonds)
calculated	2.57 A	1.698 A		1.219 A
match drawing	2 A	1.7 A	1.74 A	1.25 A
possible state	{B}, {C}	{D}	{E}	{A}

The possible molecular structures of the different states of O_2 molecules are shown in Figures [9.43, 9.44 and 9.45].

8. Examples of some molecular structures

Note: In the following drawings the protons and neutrons in the central polar section of the atomic nucleus are only shown.
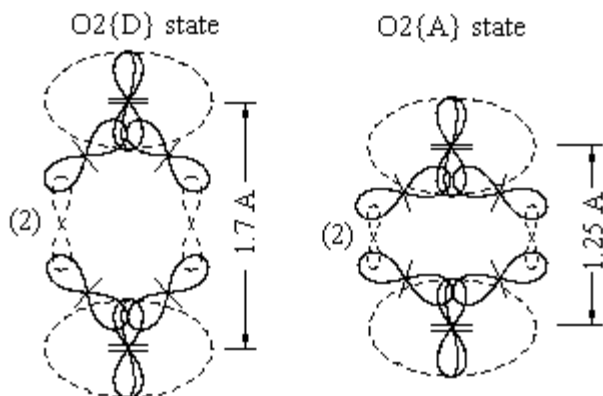

Fig. [9.43] Possible configurations of $O_2(D)$ and $O_2(A)$. {D} and {A} are states of O_2 according BSM model. The orbital planes of electrons do not lie in the drawing plane, but they are shown in this way for drawing simplification. The number in a bracket indicates the subharmonic number of the quantum orbit.
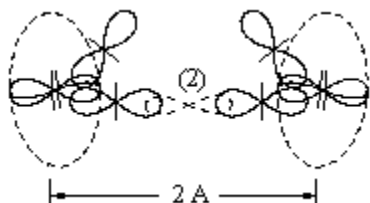

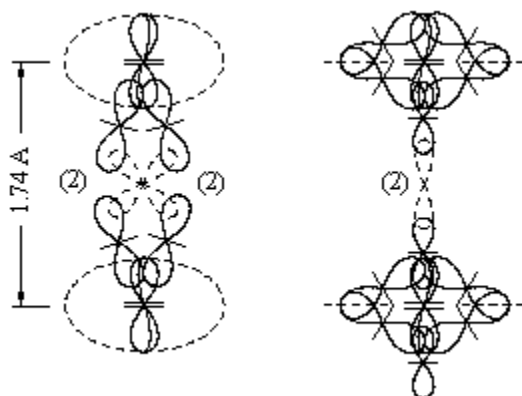**Fig. [9.44]** Possible configuration of O_2 in {B} state

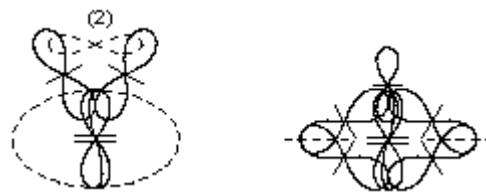**Fig. [9.45]** A possible configuration of O_2 molecule in {E} state

Fig. [9.53] Two views of the possible configuration of oxygen atom in Airglow state responsible for line emissions at 5577 A and 6300 A.
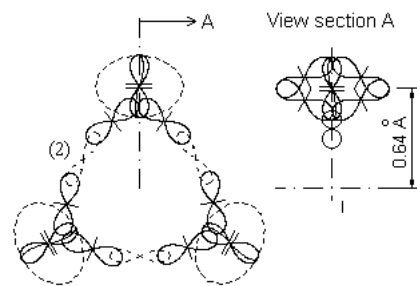
.

Fig. [9.53.A]

Ozone molecule with second subharmonic bonding orbits Every one of the three bonding orbits contains two electrons with opposite quantum mechanical spins

Fig. [9.54]

Configuration of (OH)⁻ ion. Every electronic bond orbit contains two electrons with opposite QM spins (the planes of bonding orbits are at 90 deg, in respect to the protons equivalent planes)

Fig. 9.56

One view of CO_2 molecule. The CO2 molecule possesses rotational symmetry about the polar axis due to the 90 deg rotational symmetry of C atom. If rotating 90 deg around zz axis the view of the left side will change with the view of the right side.

Fig. [9.59]
Water molecule

Fig. 9.7 Cl_2 molecule. The dashed oval is the envelope of Ne nucleus. A set of the possible quantum orbits is shown in the square box, where the number in bracket indicates the subharmonic number of electron quantum velocity. The experimental value of internuclear distance between Cl atoms is 1.98 A.
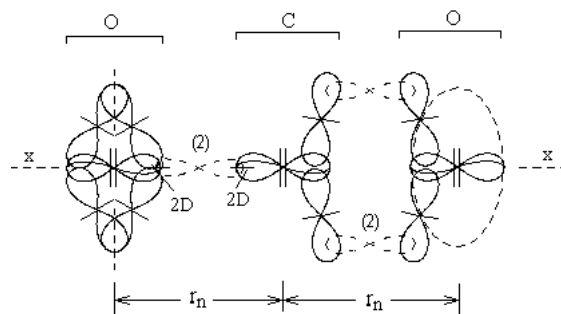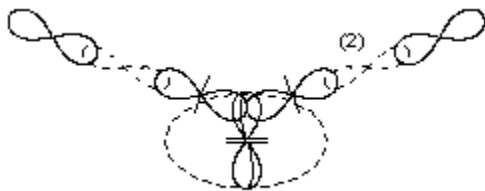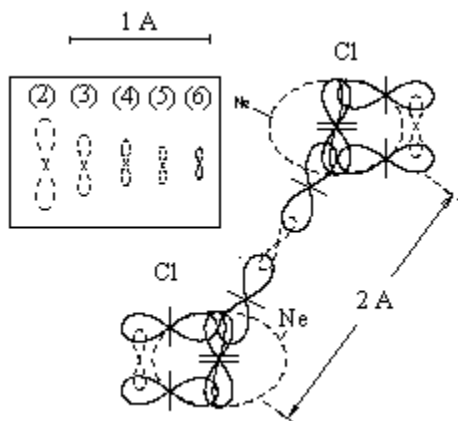
9. Rotational component in vibrational rotational spectra of molecules

The electronic type of chemical bonds allows a vibrational type of motion of the involved nuclei. The relation between the vibrational motion of a linear diatomic homonuclear molecule with electronic type of chemical bond to its optical and photoelectron spectra was illustrated in Fig. [9.15]. The vibrational levels obtained by Eq. [(9.23)] for H_2 and [(9.550] for diatomic molecules corresponds to the vibrational bands of optical spectrum for a given quantum orbit and molecular conformation. The BSM analysis leads to a conclusion that **the rotational components in the vibrational rotational spectra, according to BSM, are result of the shape distortion of the quantum electronic orbits.** There are two possible types of the shape distortion:

- a symmetrical distortion
- an asymmetrical distortion

The both types of distortion are shown respectively in Fig. [9.16], a. and b.

Fig. [9.16]
a. - symmetrical and b. - asymmetrical distortion of the bonding orbit

The vibrational motion of linear diatomic molecules involves symmetrical distortions of the bonding orbits. For molecules with two binding orbits one of the bonds is a point of rotation at any moment (contributing to Q branch), while the other undergoes a symmetrical distortion (contributing to P and R branches) and they change alternatively. The effect of the distortion of the bonding orbit and its signature in the vibrational-rotational spectrum is illustrated by Fig. [9.17].

Fig. [9.17]
Section of three consecutive levels of the vibrational
 ladder with fine structure levels from the bonding
system frequency set. In the right side the corresponding optical spectrum from transition between these levels and the lowest level is shown

The vibrational motion in bent molecules involves additional asymmetrical distortion of the binding quantum orbits. This effect contributes to folded P or R branches in some molecules with bent shape.

All atomic nuclei possess twisting around the polar axis, due to the proton twisting. Therefore, in a confine motion in CL space they perform a rotational motion simultaneously. This rotation contributes to the pure rotational spectrum.

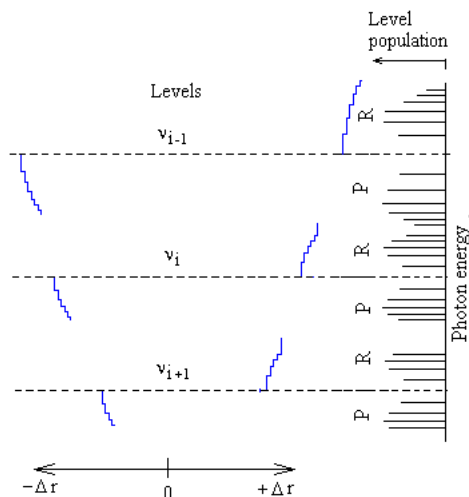## 10. Structural and angular restrictions of the atomic positions in the molecules when connected by electronic bonds

10.1. Restrictions from atomic nuclear configuration

The provided considerations in §5, §6 and §7 demonstrate that the structural and angular restrictions reduce significantly the degree of freedom of the atoms connected by electronic bonds. The same restrictions are also responsible for the molecular bending. These restricting features are not apparent from the Quantum mechanical models of the atoms.

The mentioned considerations are not valid for ionic molecules since they are not connected by electronic bonds but by attractive forces between oppositely charged ions. Their internuclear distances are also larger and they exhibit different physical properties. Consequently they are not able to possess the presented above of vibrational motion in which the quantum orbits play important roles. For this reasons the ionic compounds don't have vibrational rotational spectra. Only separated ions are able to provide ionic line spectra.

The following conclusion is valid only for chemical compounds with electronic bonds, but not for compounds with ionic bonds.

- **The degrees of freedom of connected atoms in molecules by electronic bonds are reduced by structural restrictions and limited angular freedom of the valence protons. This restrictions are defined by the nuclear configurations of the involved atoms.**

10.2. Restrictions from spin-orbital interactions

If not taking into account the implemented He nucleus and the polar electrons, every single proton in the atom has own electron, connected to the free proton club (that is not polar attached). Some of these proton clubs, however, are GBclp or EB bonded in pairs. For EB bonded protons the two electrons with opposite QM spin circulate in a common orbit whose plane is almost parallel to the polar atomic axis. For GBclp bonded protons the two electrons with opposite spin circulate in a common orbit whose plane is almost perpendicular to the polar axis. In both cases, the common quantum orbit passes through the clubs of the protons. The orbital trajectory is well defined by the proximity E-field of the involved protons. The positions of GBclp protons are strongly fixed, while the EB protons are weakly fixed by the quantum orbits. Any fixed orbit may not lye in a plane but it is quite close to a fixed equivalent orbital plane that gets a proper symmetrical position in respect to the polar nuclear axis. From above mentioned consideration it is evident that the quantum orbits connected to BGps, GBclp and EB type of bonds have fixed orientation of their equivalent planes. These fixed positions are much stronger held in comparison to the orbital plane positions of the chemical bonds.

Table 2 provides the number of different type proton bonds in the nuclei of some elements and the total electrons with commonly aligned equivalent orbital planes.

Table 2.

Atom	GBclp	EB	N_e
C	0	0	2
N	0	1	2
O	2	0	6
P	4	1	10
S	4	2	10
Cl	4	3	10
Ca	8	0	18
Fe	8	0	18
Cu	8	4	18

where: N_e - is the number of electrons with aligned equivalent orbital planes.

In the analysis provided in Chapter 8 and 9 of BSM it is found that two of the external shell protons of the oxygen atom are GBclp bonded. The signature indicating such type of bonding appears in the first ionization potential trend as a function of Z-number and also in the photoionization poten-

tial of the oxygen (known as autoionization feature). The nuclear structure of Oxygen is illustrated in Fig. 7. In the right part of the drawing, the common positions of the fixed electron orbits are shown as viewed from the polar axis. The projections patterns of the two polar orbit electrons (1s electrons according to QM model) are shown by different colours. Their similar patterns exhibit angular rotation around the polar axis due to the nuclear twisting of the atomic nucleus. This feature, valid for all atoms, is a result of the proton twisting. The GBclp bonded protons (deuterons) are shown in the plane of drawing while the valence protons (deuterons) are closely aligned to a perpendicular plane, but shown at oblique angles for a drawing simplification purpose.
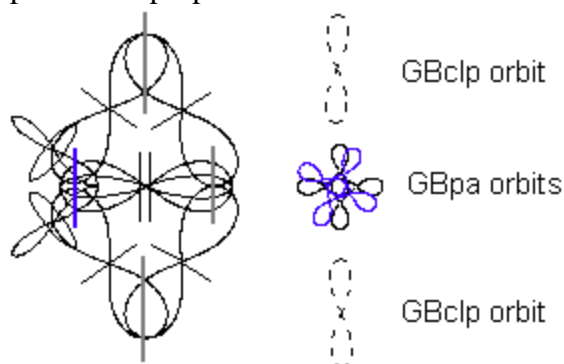

Fig. 7. Nuclear structure of the Oxygen atom

The stability of such nuclear configuration with two GBclp pairs is evidently a result of the nuclear symmetry in which the two polar electrons (from 1s shell) have strong influence. This configuration provides much larger angular freedom of the two valence protons that may explain the large chemical activity of the Oxygen atom.

11. New method for analysis of the biomolecules with identified structure and composition.

11.1. General considerations

The 3D structures and atomic compositions of many biomolecules now are well known. In such structures, the individual atoms are identified as nodes with known coordinates. The angular coordinates of their chemical bonds are also known. This information is sufficient in order to replace the nodes in the 3D structure of any large molecule with the physical models of the atoms according to

BSM concept. If the BSM models are correct, their spatial configuration and angular bond restrictions should match the 3D structure of the biomolecules. Once the BSM models are validated and corrected if necessary, the complex biomolecules and any macromolecule with known shape could be studied from a new point of view. The application of the BSM models, for example, allows the identification of the positions of all orbits. This includes the nuclear and the chemical bonds electronic orbits. Then the conditions for possible interactions, modifications and energy transfer could be analysed at atomic level.

11.2. Ring atomic structures in organic molecules.

Most of the organic molecules contain ring atomic structures. The molecule of benzene could be considered as a simple example of a ring structure. The biomolecules posses usually possess a large number of ring atomic structures. Fig. 8. shows the 3D molecular structure of aspirin where the ring structure of 6 carbon atoms is similar as in benzene. .
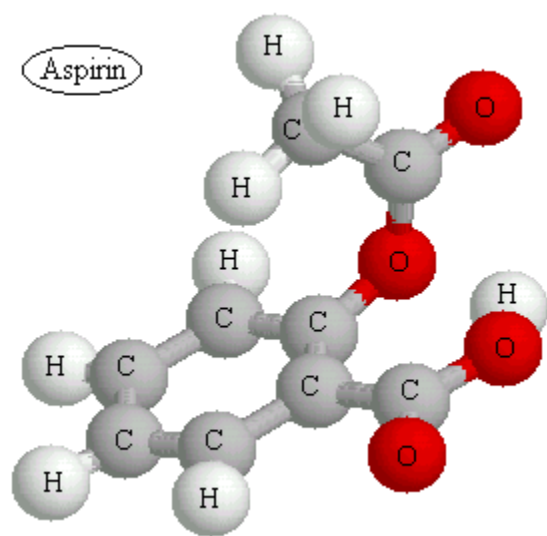

Fig. 8
3D structure of the molecule of aspirin (PDB file aspirin visualized by Chime software)

Fig. 9 shows the same structure of aspirin at atomic level by application of BSM atomic models.
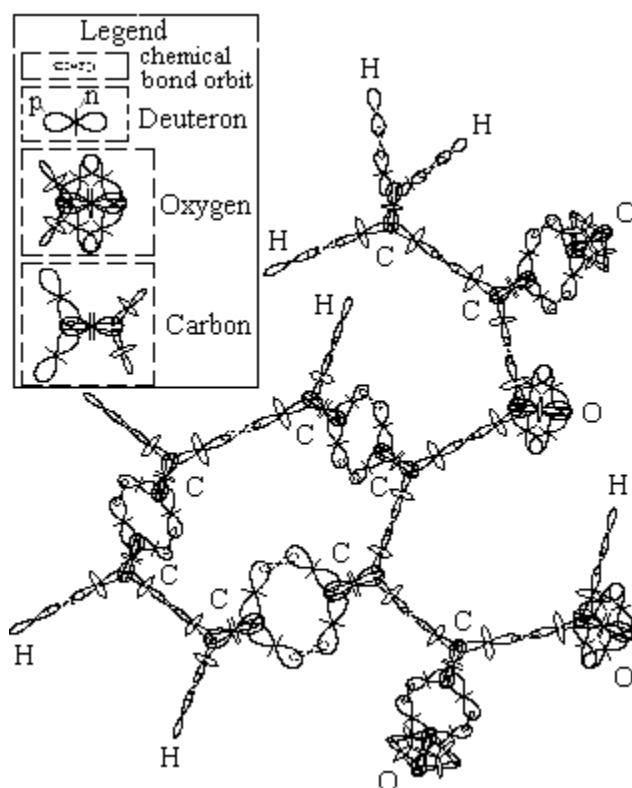

Fig. 9 3D structure of aspirin by BSM atomic models

The single atoms Deuteron, Oxygen and Carbon and the size of quantum orbit of second subharmonic are shown in the left upper corner. The valence protons (deuterons) of the oxygen atom are in fact in a plane perpendicular to the plane of EB bonded protons (deuterons) but they are shown with reduced dimensions in order to imitate an oblique angle in 3D view. The same is valid also for the valence protons of the carbon atom.

In Fig. 9 the electronic orbits providing chemical bonds are only shown. For molecule with known 3D structure and composition the common positions of all electronic orbits with their equivalent orbital planes are identifiable. It is clearly apparent that the 3D structure of the molecule is defined by the following conditions:

(a) a finite size of the involved atomic nuclei

(b) an angular restricted freedom of valence protons

(c) a finite orbital trace length defined by the quantum conditions of the circulating electron

(d) orbital interactions

(e) a QM spin of the electron (the motion direction of the electron in respect to the proton twisting)

The QM mechanical models of atoms are mathematical models in which the features (c), (d), and (e) are directly involved, while the features (a) and (b) are indirectly involved by the selection of proper wavefunctions. In this process however some of the spatial and almost all angular restrictions are lost. Let emphasize now the difference between the suggested BSM models of atoms and molecules and the QM models:

- QM model: the electrons participating in chemical bonds are orbiting around both point-like nuclei, i. e. they are not localised

- BSM model: the electrons involved in the chemical bonds are localised

- QM model: the chemical bond lengths are estimated from the electron microscopy assuming the planetary atomic model in which the larger electron concentrations are centred around the poinlike nucleus

- BSM model: the chemical bond length may need re-estimation, because the orbits of the chemical bond electrons do not encircle the bound atomic nuclei.

- QM model: The length of C=C double valence bond is estimated as 1.34 A (angstrom), while for a single valence C-C - as 1.54 A. However, these lengths show a small variation in the same ring groups included in different biomolecules.

- BSM model: the length of single C-C bond may vary only by the subharmonic number of quantum orbit, while the length in a double C=C bond is additionally dependent of the angular positions of the valence protons.

The adopted and existed so far concept of circling delocalised electrons for explanation of the equality between single and double bonds in benzene molecule is not logical from a point of view of BSM model. This is quite important for unveiling some of the specific properties of the ring structures in the biomolecules.

Ring structures are very abundant in many biomolecules and they are very often arranged in particular order along their chain. DNA and proteins contain large number of ring structures. Fig. 10 shows the spatial arrangement of ring atomic structures in a portion of β–type DNA. The posi-

tions of some (O+4C) rings from the deoxyribose molecule that is involved in the helical backbone strands of DNA are pointed by arrows.
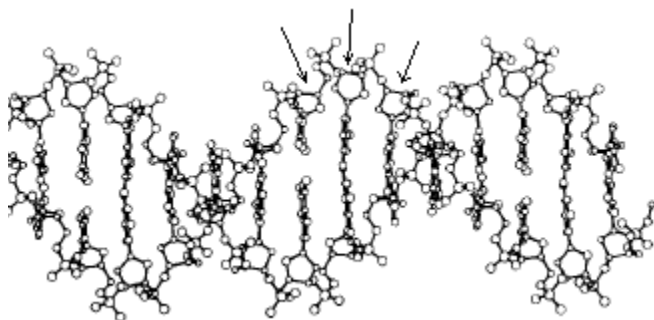

Fig. 10 Part of DNA structure with indicated positions of some of (O+5C) atomic rings

Fig 11. shows the ring atomic structure (O+4C) from the DNA strand.
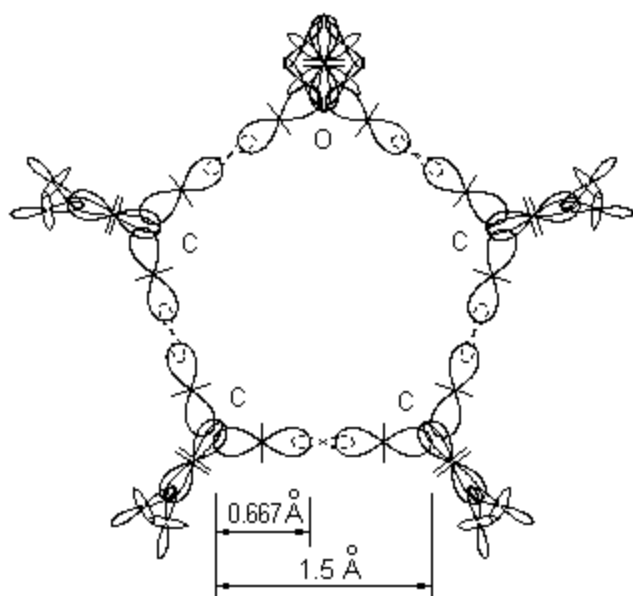.

Fig. 11. Ring atomic structure from the deoxyribose molecule involved in DNA strand

The deuterons involved in the ring structure shown in Fig. 11 practically have some small twisting, but the quantum orbit of single valence bond also could be twisted. This feature gives some freedom for formation of ring structures of different atoms. The rotational freedom of the single valence bonds, however, may be accompanied by some stiffness that increases with the degree of the orbital twisting. Some of the atoms of the ring structure are also

connected to other external atoms. All this considerations provide explanation why the ring structure (O+5C) connected to the DNA strand is not flat but curved.

11.3 Weak hydrogen bonds

It is known that a weak hydrogen bond is possible between two atoms, one of which does not possess a free valence. The bond connection is a result of orbital interactions. In such aspects the hydrogen bonds connecting the purines to pyramidines in DNA molecule are of two types: <N-H...O> and <N-H...N>, where the single valence electronic bond is denoted by "-" and the H-bond is denoted by "...". The BSM concept allows to find the possible orbital orientation for such type of bond. This is illustrated by Fig. 12.

Fig. 12. Two types of hydrogen bonds

In a hydrogen bond of type N-H...O the plane of electronic orbit of hydrogen appears almost parallel to the commonly oriented nuclear orbits of oxygen atom in which six electrons are involved (see Table 2 and Fig. 6). In a hydrogen bond of type N-H...N the plane of electronic orbit of hydrogen is almost parallel to the equivalent planes of the two polar orbits of N in which two electrons are involved.

It is evident that the hydrogen bond is characterized by the following features:

- the connection is a result of common orbital orientation

- the H-bond requires critical range of distance
- the H-bond allows a rotational freedom in a limited angular range.

This three features allows the DNA molecule to possess excellent folding properties.

11.4. Hypothesis of energy storage mechanism in molecules possessing ring atomic structures.

It is well known from the atomic spectra, that only the alkali metals (Group I) and the positive atomic ions with a single valence electron possess atomic spectrum that could be described by the Bohr atomic model. For elements with more than one valence electron, the principal quantum numbers exhibit more than one energy level (degenerate levels), due to the spin orbital interactions. The signature of this feature is apparent from the Grotrian diagrams for atomic spectra. This spin-orbital interaction from a point view of BSM atomic models is discussed in Chapter 8 of BSM. The analysis leads to a conclusion the pumped CL space energy is not emitted in full, after an orbiting electron is dropped to a lower quantum level. Part of the pumped energy is preserved by the atomic nucleus and redirected to the valence proton, whose quantum orbital plane is parallel to the orbital plane of the consideration. The physics of this effect is explainable if considering the total energy balance including IG field. The latter controls the proton's proximity E-fields distribution, that from his hand defines the orbital conditions of the electron. Therefore, the redirected energy provides some shift of the energy levels, but the effect is stronger for the lower states closer to the ground state of the series (Balmer series has own ground state, according to BSM model). The physical explanation of this effect allows making a conclusion that the released energy prior to formation of a photon is **preferentially guided by connected structures of protons (deuterons)**. Applying the same considerations for the ring atomic structures there must therefore be a guiding energy process between the atomic nuclei or protons involved in the ring. Such consideration leads to the following conclusion:

In proper environments, the ring atomic structures in organic molecules may have ability to store energy as an exited state rotating in the ring loop.

The effect of the rotating excited state is possible due to the consecutive re-excitation of the electrons in the separate bonding orbits in the ring. This effect is not apparent by the Quantum mechanical model, where the wavefunctions are complex envelope around the whole nuclei of the involved atoms. However, it is a known fact that the bonding strengths between atoms involved in a ring atomic structure are stronger than between same atoms when not participating in such structure.

Evidently, the condition of rotating excited state in a ring structure could be obtained only for equal energy level differences. Such concept allows considering excited states not only from same valence bonds but also from single and second valence bonds as well. From the other side, for a ring structure containing more than two bonds of same valence, excited states may preferentially exists between the same valence bonds. In case of aspirin, for example, such conditions exists for three pairs orbits of second valence and three pairs orbits of single valence bonds. If considering also the fixed nuclear orbits of the atoms in the ring then twelve polar electrons could be also involved in a ring storage effect. Theoretically they may store a much larger energy not only due to their number, but also due to the larger transition energies.

In proper environments, the stored energy in the ring structures of the biomolecules may have the following features:

- a stable cycle of exited state rotation due to a stable finite time of single excited state

- a possibility for interactions with properly oriented neighbouring ring structures in the moment between two consecutive excited states (conditions for synchronization between the rotating states of neighbouring rings)

- a cascade type of energy transfer

Many of the building blocks of the biomolecules or reagents contain number of single or attached rings. For example Adenine (2 attached rings), Guanine (2 attached rings). Vitamin D contains one single and two attached rings. Alpha and Beta tubulins contain groups of: GDP (one single and two attached rings), GTP (one single and two attached rings), TAXOL (4 single rings). The ster-

oids hormones contain usually four attached atomic rings. The ATP, an important energy carrier in the cells contains one single and two attached rings. It is quite logical to consider that the energy rotating cycles in the attached rings are mutually dependable so they must be synchronized. Then it is logically to expect that the attached rings may have an increased ability to hold a stored energy in case of environment change.

11.5 Hypothesis of energy flow through the chain structure of the biomolecule.

11.5.1. Energy flow in DNA molecule and its effect on the higher order structural characteristics.

 For long chain biomolecules, like DNA, the ring atomic structures are characterised by few additional features:

(a) a strong repeating order

(b) a strong orientation in respect to the host strand of DNA

(c) a strong orientational order of the neighbouring rings along the helix

These features are well known and can be easily visualized when rotating the 3D structure of DNA (by programs like: "chime" "Rasmol", "protein explorer" etc.).

The consideration of cascade type of excited state transfer could be applied not only for a ring atomic structure but also for a long chain molecule built of repeatable atomic structures connected by electronic bonds. In this case some more complicated but mutually dependable mechanisms are involved. The following analysis tries to unveil such mechanisms. Let considering for this purpose one of the backbone strands of DNA. Fig. 13. illustrates the connection path of the electronic bonds in the strand. Three important features are apparent for every repeatable cascade:

(d) the bond connection path is formed by deuterons or protons connected by electronic orbits

(e) the bond connection path passes through one C-C bond from the (O+5C) ring.

(f) all bonds involved in the bond connection path are single valence

Fig. 13. Bond connection path through a DNA strand The connection path corresponding to one cascade of the nucleotide is denoted by a thick green line

It is reasonable to expect that the long chain of single valence bonds may provide conditions for cascade excited state transfer in one direction. The time of every excited state is determined by a quantum mechanical consideration - the lifetime of the spontaneous emission. Keeping the small distance between the neighbouring electronic bonds, the transfer time between two consecutive excited states (with a light velocity) is practically almost a zero. Then the time dependence between the two energy process (a cascade energy transfer and cycle period of energy rotation in the ring) is easily obtainable. The bonding path of one cascade contains six bonds total in which one C-C bond from the (O+4C) ring is included. This ring involves five bonds. Then one may consider that the following condition is valid:

$$0 < (T_R - t_c) < \tau_{av} \tag{1}$$

where: t_c - is the time transfer interval for one cascades of nucleotide estimated by the sum of lifetimes of excited states in involved bonds, T_R - is the cycle time of the rotating state in the ring, τ_{av} - is the average lifetime for a single bond.

The expression (1) means that the cascade transfer and ring cycle are mutually time dependable processes, so they should have proper **phase synchronization.** Additionally, all parameters of Eq. (1) are dependable from the temperature, but in a different way. This will impose a limit temperature range for successful phase synchronization.

Keeping in mind the features (a), (b), and (c), the rotating energy states in the ring could be commonly dependable.

The whole mechanism will be characterised by the following features:

(k) the rotated excited states in (O+5C) rings will possess one and a same handedness determined by the direction of cascade energy flow through the strand to which they are attached

(l) the rotating energy states are phase synchronized along the DNA strand

(m) the rotating energy states sustain the tendency of unidirectional cascade energy flow through the DNA strand

(j) the whole mechanism will work at optimum temperature and limited temperature range both defined by the conditions of optimal phase between the cascade energy transfer and the ring energy cycle.

It is apparent that the commonly dependable features (g), (h), (h) and (j) will lead to a self-sustainable mechanism.

Let analyse now the conditions that may support the tendency of unidirectional energy transfer. For this reason we will consider a small portion of DNA ignoring it supercoiling. In such case it could be regarded as a linear type DNA. Two structural features of Beta type DNA that might be related to the tendency of unidirectional energy transfer:

- It is well known that the nucleotide arrangement in DNA is antiparallel, so the same definition is valid, also, for the bonding paths through the two strands.

- The DNA double helix is characterised by a minor and major grove. This means that one of the helix is slightly axially shifted in respect to the other.

The concept of unidirectional energy flow through the DNA strand could be investigated if associating it with the magnetic field of a solenoid. In such approach, the double helix configuration of DNA could be regarded as two parallel solenoids with a common axis. Now let consider that the cascade energy flows through the both strands are in opposite (aniparallel) directions. This will corresponds to opposite currents through both solenoids. In such case, the magnetic lines in the internal region of the solenoids will have antiparallel direc-

tion, while the external magnetic lines will be closed in proximity of both ends of the solenoids.

Let call this type of field a "**complimentary compensated solenoids type**". The magnetic lines of such field are schematically illustrated by Fig. 14. The two solenoids that simulate the two strands are shown by green and red. Their field lines shown as dashed lines are antiparallel inside the solenoids, while they are connected in proximity at the both ends.

Fig. 15. Association of energy flow conditions between DNA strands with complimentary compensated solenoids. The magnetic field lines close in proximity at both ends of the solenoids. The current directions in both solenoids are opposite (shown by black arrows)

If attempt to separate the both solenoids, they will opposed.

The analysis of magnetic field with such spatial configuration leads to the following additional features:

(h) The configuration of the associated magnetic field is independent of the secondary (supercoiling) shape of DNA

(i) Such type of magnetic field will provide an additional strength of the connections between the both strands. It will oppose the separation between the strands because this leads to increase of the close path lengths of the magnetic lines

(j) For a small portion of DNA molecule the complimentary compensated solenoids type of field is axially symmetrical.

The provided considerations may put also a light about the hydrophobic mechanism existing in the space between the two DNA strands. The two bond angles of water molecule are illustrated in Fig. [9.59] where the positions of the orbits of the two valence electrons are also shown. If a water molecule is placed inside the symmetrical field of the compensated solenoids, the angular positions

of the valence electron orbits evidently will be in a conflict with the solenoids field. The interaction of the orbiting electrons with such field may provide expelling forces for such type of molecule. This might explain the hydrophobic environments of the internal region of DNA between the two strands. The hydrophobic environment is quite important for H-bondings between the purines and pyrimidines.

The analysis of compensated double solenoid model for the energy flow through DNA leads to the following conclusion:

(A). The DNA double helix molecule could be easily folded in any shape under influence of external factors.

The external factors could be different kind of proteins.

11.5.2. Magnetic field conditions for proteins.

It is well known, that in proper environments the proteins, that usually possess a complex tertiary structure, preserve their native shape. The linear DNA, from the other side, when it is free of bending proteins, does not exhibit such a feature. The main reason for the different behaviours of the proteins and the DNA of linear type perhaps is a result of the structural differences between them. The protein is a long single strand molecular chain with diversified sequences of aminoacids. The protein backbone does not contain low order repeatable structures as the DNA nucleotide. It may contain, however, higher order repeats, that may form some helices with small number of turns or other spatial configurations. In such arrangement the conditions for H-bonding are significantly reduced. All these structural differences indicate that we could not apply the concept of the complimentary compensated solenoids for the proteins, as for the analysis of DNA.

The conclusion, that the diversified sequence of the aminoacids is one of the reason for the different higher order shape of the proteins is supported by the analysis of the shape of the tRNA

molecule. Its shape and atomic composition is shown in Fig. 16.

Fig. 16. tRNA molecule. (a) - real shape, (b) plane drawing, showing the loops and base pairs

The tRNA molecule possesses a single strand of about ... base pairs but the repeating order of the nucleotides is similar as in the DNA molecule. Its single strand arrangement obtains a stable shape of "cloverleaf" demonstrating in such way a tendency for arranging parts of the long single strand in proximity.

In such arrangement, the unidirectional magnetic field through the single chain of tRNA becomes of type closer to the complimentary compensated solenoid, so the principle of shortest magnetic lines is satisfied. The magnetic lines through the strand are connected in the proximity at the open ends and this is the area where the tRNA molecule attaches a proper amino acid.

The proteins synthesized according to the DNA code have different sequences of amino acids and exhibit a large diversity in their taxonomy. While the model of the complementary compensated solenoids is not valid for the proteins, they still could be analysed by a single solenoid model. If accepting that a unidirectional cascade state transfer is possible through the bonding path of the chain, then a single solenoid model could be used for the helices of the protein. In such aspect the analysis of secondary and tertiary structures of the proteins leads to the following considerations:

(a) Different types of secondary structures as helices, sheets, beta turns, bulges and so on provide different structures of magnetic fields.

(a) The magnetic field from the unidirectional cascade state transfer may influence the common positions of the secondary structures

(c) The bond angular positions between neighbouring atoms are restricted by the strong conditions of finite nuclear structure and restricted angular freedom of the chemical bonds

(d) Discrete type of rotational freedom with some finite deviation is possible between single valence bonds

(e) The above mentioned considerations and spatial restrictions lead to a conclusion that an overall asymmetry of the magnetic filed from the secondary structures (mainly from the helices) may exist. Then the tertiary structure may tries to restore the asymmetry of magnetic fields arisen from the diversified secondary structures by obtaining an overall symmetry at some higher structural order. Simultaneously this will be accompanied with a tendency of shortest magnetic lines.

(f) The cascade energy transfer through the bonding path of the protein chain might be accompanied with some ion current, whose energy could be also involved in the total energy balance.

The taxonomy of 3D protein structures is well described in the book Advances in Protein Chemistry (1981) by C. B. Anfinsen, J. T. Edsall and F. M. Richards.

The stiffness of the secondary order structure is larger than the stiffness of the tertiary one. This matches the strength of the mechanism involved in the restoration of the overall field symmetry. As a result every protein may have a sustainable native shape when placed in proper environments (temperature, pH, ATP).

The provided analysis helps to explain one of the problems in molecular biology, known like a Levinthal's paradox: "Why the proteins folds reliably and quickly to their native state despite the astronomical number of the possible quantum states according to Quantum mechanics?".

Now let find out how the protein may react if the condition of shortest magnetic lines is temporally disturbed by some external factor, for example, by addition of Adenosine triphosphate (ATP). The ATP carries stored energy in its rings. When

the chemical reaction $ATP + H_2O \rightarrow ADP + P$ occurs the stored energy might be induced in some rings in the protein under consideration. This may change the conditions at which the principle of shortest magnetic lines and compensated field is satisfied. Then the reaction leading to restoration of the energy balance (involving the magnetic energy) could involve some kind of change of shape and motion of the protein. This may eventually explain the protein motility in proper environments (temperature, pH, ATP concentration) that is simultaneously accompanied with temporary changing of its higher order shape.

11.5.3. Environment considerations for preservation of the native shape of the biomolecules.

Many proteins have a complex 3D structure with secondary helix and tertiary structure. They exhibit amazing tendency to preserve their 3D shape in proper environment conditions in which the temperature is one of most important factor.

The electronic bonds and hydrogen bonds allow some freedom of the 3D structure of biomolecules. It is known from the Quantum mechanics that the excitation of particular vibrational-rotational band of the molecular spectra is temperature dependant. Translated to BSM model this dependence means:

- a selection of proper subharmonic number from the available set of the quantum orbit

- a selection of proper quantum number

Consequently the complex 3D shape of the biomolecules is dependable of two main features:

(a) a proper subharmonic and quantum number of every bonding electron

(b) a same subharmonic and quantum number of the similar interatomic bonds along the molecular chain

The feature (a) provides a requirement for the absolute temperature range for the preservation of the native state of a long chain molecule, while the feature (b) put a strict requirement for a temperature uniformity along the molecular chain. This, of coarse is not the only factor. Additional factors are the interactions between the highly oriented atomic ring structures discussed in previous paragraphs and the conditions for H-bondings.

Another environmental conditions that are also important, for example, are such as the pH factor and ATP concentration. The first one may assure the proper ion current conditions (according consideration (f) in section 12.5.2), while the second one - the necessary energy.

11.5.4. Magnetic field involved in the higher order structures of DNA.

The DNA molecules of the single cell organisms are usually of circular type with a supercoiling. The DNA of eukaryotes, however, is of linear type with much more base pairs and complicated secondary and third order structures. According to the principle of the short magnetic lines and compensated magnetic field, the circular DNA should be more resistant, because the magnetic line paths are enclosed inside of the structure. This condition might be partly disturbed only during the transcription. The linear DNA, however, posses some additional properties that may facilitate the process of intermolecular DNA communications, according to a hypotheses presented below.

The length to diameter ratio of DNA is very large. It is extremely large especially for eukariotic DNA. For human chromosomes, for example, the average ratio is in order of 10^7. In order to be held in a tiny space of cell nucleus such long molecule have higher order structure, known as supercoiling. The mechanisms involved in the formation and sustaining of such a structure has not been completely understood so far. The following analysis put some light about the possible mechanisms.

Let first present shortly some of the experimental observations about supercoiling features of a long DNA. In the paper "DNA-Inspired Electrostatics" in Physics Today by W. M Gelbart et al. (2000), the authors provide a summary about one important feature of DNA. They say: "Under physical conditions (a 0.1 molar solution of NaCl), a DNA molecule takes on the form of a disorder coil with a radius of gyration of several micrometers; if any lengths of the molecule come within 1 nm of the other, they strongly repel. But under different conditions-in a highly diluted aqueous solution that also contain a small concentration of polyvalent cations - the same DNA molecule condenses into a

tightly packed, circumferentially wound torus." Fig. 17 shows the toroidal shape of DNA from the same paper, that has been adapted from O Lamber et al., (2000).

Fig. 17 Toroidal DNA condensates, Courtesy of O. Lambert et al. (2000) (Adapted from W. M. Gelbart et al., (2000).

The DNA molecule is usually negative charged, so the repels between the different part of the long chain molecule in close distance about one nm is understandable. However, why the DNA folds in such packed toroidal structure in a presence of proper polyvalent cations? This effect gets reasonable physical explanation by BSM theory if analysing the magnetic field conditions in a CL node level.

Fig. 18. Electrical field and SPM Quasisphere elongation between two parallel parts of DNA

Fig. 18 shows the electrical field intensity between two parallel parts of DNA. The left vertical scale axis shows the electrical field intensity, while the right vertical axis shows the elongation of the SPM quasispheres in the plane of drawing. One specific feature is apparent from the drawing: the elongation of SPM quasispheres (see Chapter 2 of BSM) becomes zero in the middle between the parallel strands. This is possible only due to the strong spatial orientation of the EQ (contributed to the E-field) along the parallel DNA parts. Consequently, the elongation of all SPM quasispheres in the plane passing through the parallel DNA axes is reduced to zero. Then these SPM quasispheres become of MQ type (magnetic). In the same time the SPM vector of these MQs might be synchronized, because the interacting EQs from the parallel long chains could be easily synchronized. Then the obtained in such way MQs provides excellent conditions for a permanent magnetic field. In order its direction to be permanent, however, it needs inertial type of interactions with some external current. Such current may be provided by heavy and polyvalent ions, while the masses of Na and Cl 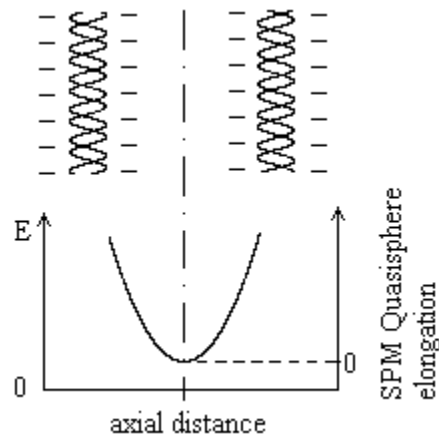are not so different and their charge is not enough large. The current flows of the positive and negative ions are expected to have different paths. This could happen if they have different masses, because they will get different centripetal acceleration in a helical trajectory. The supercoiling shape of the long DNA will provide a necessary condition for such trajectory. In the same time the condition of short magnetic lines will keep the supercoiled DNA in compact configuration, while the negative charge of DNA strands will keep the proper distance between the different parallel parts of the molecule.

The explanation of the DNA supercoiling in eukariotic cells in a natural cell environments requires some additional considerations. The human DNA, for example, is supercoiled around a protein called histon octamer. The shape of the higher order structures of DNA as a nucleosome formation,

a Chromatin and a Chromosome are presently well known. They are illustrated by Fig. 19.

Fig. 19. Higher order structures of DNA in Chromatin and Chromosome

The conclusion (A) in §11.5.1 provides an explanation why the DNA molecule is easily folded as a secondary helix around the histone octamer. The latter, evidently, provides a higher order helical shape conditions. According to the considerations in §11.5.1 and §11.5.2, the histones may also have features of energy flow. If examining the atomic structures of the histones (by using the Protein data Bank) we will find that two type of atomic rings: (6C) and (N+4C) are involved among the building atoms. A possible energy flow through the spatially arranged rings may play a role in the DNA bending and coiling around the histone octamer.

The Chromatin, known as a chromatin fibber (with diameter of 30 nm) is additionally coiled into a daisy flower shape, called a chromosome miniband. The chromosome miniband, shown in the left bottom side of Fig. 17 contains 18 loops of daisy flower shape. A stack of daisy flower minibands arranged in a superhelix with diameter about 840 nm forms a chromosome.

The discussed effect of magnetic field creation with sustainable ion current may be part of the complex mechanism sustaining the supercoiled structure of the human chromosome. The balance between the magnetic field, the ion current and the electrochemical potential will depends of the internal cell environments as in the case of the proteins. Simultaneously, the principle of the short magnetic

lines and compensated magnetic field should play also some role. When one of the both ends of the chromosome is attached to the cell the ion current and magnetic field will be stabilized, so the super-coiled shape will be stable. If the chromosome, however, is not attached by some reason, a small change in the ion current will cause a reaction of the magnetic field. This may invoke a shape change and a motility of the chromosome.

11.6. Hypothesis about the role of DNA in the cell cycle synchronization mechanism

11.6.1 General considerations

The cell cycle synchronization is an important factor for a normal organ formation in the growing multi-cellular organism. One simple example demonstrating such importance is the eye formation. Some not synchronized cell division in early phase of eye formation may lead to significant defects. However, how the enormous number of individual cell know when exactly to enter into mitosis? If only individual clocks mechanisms in the cells are involved, they could be asynchronized after a number of cycles. A synchronization by chemical messengers through the bulk of enormous amount of cells is also not quite convincing.

It is reasonable to expect that DNA might be involved in the cell cycle synchronization. The analysis of DNA at atomic level by BSM concept led to formulation of hypothesis about electromagnetic intercommunication of DNA molecules located in different cells of the same type. The proposed hypothesis suggests a physical mechanism that might be involved in the synchronization process.

Let use the concept of complimentary compensated solenoids involved in §11.5.1., but regarding the both complimentary parts of this system as separate helices. In this case, they could be considered as two solenoids serially connected in circle. Then the direction of cascade energy transfer through both strands of DNA (corresponding to the two separated solenoids) could be in clockwise or counter clockwise conditions. This will define two different directions of the magnetic lines. Let suppose, that the obtained magnetic field is involved also in some interaction processes in the cell, so it could not be reversed spontaneously.

This means that the direction of the cascade energy flow in respect to the helical direction will be kept stable. Let denote the direction of a stable energy cascade through one strand to be +z. This direction regarded as axis +z in fact is not a straight line, but helix geometrically centred with one of the DNA strands. The stable energy flow through this strand will obviously influence the direction of the rotating energy states in the attached (O+5C) rings. Thus we may accept that they all have a clockwise direction coinciding with the rotating direction of the running energy cascade through DNA strand along +z axis. In other words all stored energies in (O+5C) rings have the same handedness. Note that the definition of handedness is referenced to the direction of the cascade energy flow.

Let now pay attention about the energy storage capability of Purines and Pyrimidines involved in DNA. The pyrimidins Cytozyn (C) and Thymin (T) have single rings (2N+3C) with electronic bond connection to the DNA strands. The Purines adenine (A) and Guanine (G) both have two attached ring structures (2N+3C) and (2N+4C) that are also connected to the DNA strands. Because, the single rings of C and T are the same as the attached rings of A and G, we may accept that they carry one and a same amount of stored energy.

The Purines and Pyrimidines have stronger bond connections to their own strand, than between themselves as base pairs. The handedness of their stored energies could be also influenced directly by the handedness of the energies in the (O+5C) rings from the strands. Using the same logic, the (2N+3C) rings should get the proper handedness from the strands to which they are strongly connected. The attached to them (2N+4C) rings however will get a complimentary opposite handedness.

Now let consider the normal situation, when the both strands of DNA are closely spaced in a shape of double helix. If aligning the DNA along a new defined axis +Z, the rotated energies in the rings connected to one selected strand, say a first one, will have a clockwise rotation, while from the second one - a counter clockwise. Consequently, when introducing a common direction axis (+Z) for both strands, the energies from (O+5C) connected to the two strands of DNA will look as they have different handedness. (In the further analysis, the

common +Z axis will be considered for both strands).

Table 3 provides the handedness of the stored energies for all types of rings in DNA molecule, as a result of the above analysis. The stored energy handedness is referenced to a common axis Z+ of the DNA molecule.

Energy and handedness states   Table 3

====================================

strand A	strand B	Energy states for
$E_S/|\backslash$	$E_S\backslash|/$	(O+5C) ring
$(E_1/|\backslash)(E_2\backslash|/)$ ------- $(E_1\backslash|/)$		A---T and G---C
$(E_1/|\backslash)$ ------- $(E_2/|\backslash)(E_1\backslash|/)$		T ---A and C---G

Notations:

/|\ and \|/ - two state of handedness

ES - a rotating state energy in (O+5C) ring

E1 - a rotating state energy in (2N+4C) ring

E2 - a rotating state energy in (2N+3C) ring

----- a connection by hydrogen bond

$(E_1/|\backslash)(E_2\backslash|/)$ - energy states with complimentary handedness in attached rings

Let examine, now, how the stored energies in the rings of different types could be influenced from some change of cascade sequence. The energies of (O+5C) rings can be stronger affected by a change in the energy cascade flow through the strand, because the strand bonding path passes through C=C bond of every ring. The stored energies in single (2N+3C) rings could be affected by the change of the cascade type energy flow through (O+5C) rings. The stored energies in the attached rings (2N+3C) and (2N+4C), however, is of complimentary type, so it is more resistant to the mentioned above energy flaw changes.

Summarizing the above considerations we may conclude:

(1) The stored energy sequence in (O+5C) rings (with unit value of E_S) is strongly influenced by a change in the cascade energy flow through DNA strands

(2) The complementary energies $(E_1/|\backslash)(E_2\backslash|/)$ in the attached rings are more stable than the energy E_1 in the single ring.

(3) A change of energy sequence in (O+5C) rings could influence stronger the stored energies in the single (2N+3C) rings than in the (2N +4C) rings.

(4) The energies E_1 and E_2 from connected by H bonds A--T and G--C have always the same handedness.

Now, let consider that the DNA strands are opened in one end only. In such case the paths of the magnetic lines is increased at this end. It is known from the physics that if some alternative field components appear in such conditions, some energy will be emitted as EM waves. At this point, however, we must consider some specific features of the double helix structure DNA:

The (O+4C) rings, arranged in a helix, contains equally spaced gaps. Having in mind the enormous number of these rings, the cascade energy transfer will have a very large unidirectional component but quite a small alternative component for one clock. Then it is reasonable to accept that the generated magnetic field will have the same unidirectional feature like the field from the energy cascade through the strands. This means that every emitted pulse will have energy of $2E_S$.

When considering the energies of single rings (N2+C4), however, the emission conditions are different. They do not form uninterrupted sequence along the chain as the (O+4C) rings, so the sequence of the released E_1 energies can not possess an own permanent component. This might affect the preferred direction of the magnetic field generation. The helicity of DNA and higher order helicity of chromatin and chromosome with some complimentary ion currents may also provide conditions of energy release from (O+4C) rings in one and a same direction for both strands. It is reasonable to accept that the emitting direction could follow the direction of emptying the energies of (O+4C) rings. Let considering that this direction corresponds to the introduced +Z axes. Fig. 20 illustrates the sequence of emptying the stored energies in (O+4C) rings (with individual energy E_S) and (2N+4C) rings (with energy E_1). The energy status and the direction of energy emission are shown for two consecutive clocks (i) and (i+1). The energies stored in the two attached rings (2N+4C) and (2N +3C) are not shown in the figure, but they are always complimentary to the (O+4C) rings.
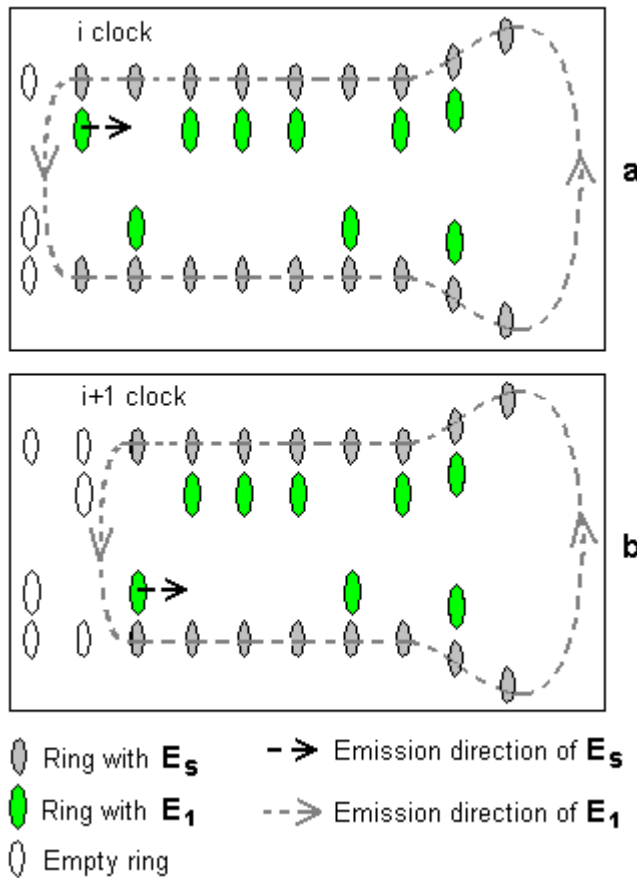
Fig. 20 Energy status and direction of energy transfer for two consecutive clocks. The emitting direction is along +Z axis

The handedness of all E_S energies in respect to the direction of the permanent magnetic field (defined by the cascade energy transfer through the bonding path) indicated by arrows in a dashed line is one and a same. When emitted by the common +Z direction the corresponding E_S energies contribute to a common $2E_S$ pulses. For E_1 energies, however, the emission conditions are different because they do not have a stable unidirectional sequence. Then considering the energy emptying direction +Z the handedness from E_1 belonging to the different strands are different (clockwise or counterclockwise in respect to +Z axis). Let considering:

(a) The E_1 energies with clockwise handedness in respect to +Z axis provide a photon sequence with a clockwise phase difference between the photons.

(b) The E_1 energies with a counter clockwise handedness in respect to +Z axis provide a photon sequence with a counterclockwise phase difference between the photons.

(c) The emitted photons of E_1 energies from the same strand are entangled with preserved phase difference. The phase advance in one strand (with +Z orientation of its cascade energy) will have a clockwise phase sequence, while from the other strand it will have a counter clockwise.

(d) Anyone of the both sequences of entangled photons contains embedded information about the A--T and G--C sequence of DNA referenced to one strand.

(e) The energy of entangled photon sequence is less dispersive in conditions of intercellular transmission.

(f) The probability of absorption of the entangled photons is much higher if meeting a similar spatially arranged atomic rings.

(g) If the process of DNA energy release is invoked not by internal factor, but from externally induced synchronization, it might have some phase delay, due to a missing of the initial synchronization sequence.

The photon entanglement is observed in lasers. Firstly, two entangled photons have been observed few years ago. Observation of three entangled photons has been published by Zelinger group (D. Bouwmeester et al, 1999) The authors express opinion for "entanglement between many more particles". The same group later reported observation of four entangled photons. Observations provided with entangled photons show that they fight the diffraction limit valid for a single photon. This may provide explanation of the mentioned above feature (e).

It is reasonable to consider that conditions of uniform temperature and proper spatial arrangement of the ring structures in DNA may provide the possibility for multiple photon entanglements in the described above mechanism. It is known from the single mode narrow line emitting lasers that their coherence time is quite long. Let for example accept that the coherence time in the DNA emitting process is in order of 1E-12 sec. If an average lifetime for a single bond is about 1E-14 sec, then the time between two E_S clocks is 6E-14 sec (six bonds). In this case, the entangled sequence will in-

clude a binary code corresponding to 600 E_S clocks. Such binary code corresponds to 600 bp (base pairs) and involves 200 codons.

Now let pay attention about one particular problem related to DNA investigation, known as a **C value paradox**.

A substantial fraction of the genomes of many eukaryotes is comprised of repetitive DNA in which short sequences are tandemly repeated in small to huge arrays.

Tandemly repetitive sequences, known as "satellite" DNA's are classified into three major groups;

-satellites - with repetitive lengths from one to several thousands base pairs.

- minisatellites - repetitive arrays of 9 to 100 bp, but usually 15 bp, generally involved in mean arrays lengths of 0.5 to 30 kb.

- microsatellites - repetitive arrays of short 2 to6 bp found in vertebrate, insect and plant genomes.

The code of repetitive sequence does not encode amino acids. The percentage of this non-informative DNA increases significantly with organism complexity but depends also of other factors. Among them are the living environment conditions of the species.

From a point of view of proposed hypothesis, the C value paradox obtains quite logical explanation:

(h) The repetitive sequences in DNA code provide repetitive synchronization code that may increase reliability of the DNA intercellular communication.

A large number of not discussed here diversified features of the DNA redundancy in different organisms and species could find a logical explanation from the point of view of feature (h).

For example, the shown below repetitive sequence in DNA from Drosophilia corresponds to the following binary codes embedded in two entangled photons, related to the two strands:

(AATAT)n, where n - is number of repeats
from DNA strand 1: (00101)n
from DNA strand 2: (11010)n

If the emitted entangled photon from strand 1 contains CW circular phase sequence of the code, the emitted entangled photon from strand 2 will contain CCW circular phase sequence of the complimentary code.

It is evident that the entangled photons carry embedded code that is dependable of both: the amino acid code and the redundancy code. This dependence may eventually play a role in the immunological response to transplanted tissues or organs. The redundancy code greatly increases the probability of successful synchronization. Then it is reasonable to expect a large abundance of repeatable code near the end side of the linear DNA in eukariotic cells.

11.6.2. Time sequence in the energy read-out process of DNA and its possible relation to the cell cycle synchronization.

Let consider some initial state of DNA molecule when all rings are charged with their normal energies E_S, E_1 and E_2. In some moment invoked by internal or external triggering the stored energies start to clock out with synchronization sequence E_S and two entangled photon sequences. Ones this process is started it will be self sustained until all E_S energies states are read-out. We may call this a read-out process of DNA. The time duration (t_{total}) for DNA read-out should be

$$t_{total} \approx 6t_{av}\frac{DNA \text{ length}}{0.34 \text{ nm}} \qquad (2)$$

where: t_{av} - is the average lifetime of excited states in the bonding path of DNA strand, 0.34 nm is the distance between the rings of the neighbouring base pairs.

The total read-out time is very short. For DNA with length of 1 m and $t_{av} \sim$ 1E-14 s the read-out time is only 0.18 ms.

After the DNA is read-out, all E_S energies are emitted. The E_1 energies only of the T and C are emitted, but the complementary state energies E_1 and E_2 of A and G are preserved due to the attached rings. This invokes some type of asymmetry between connected Purines and Pyrimidines by H-bonds. Such conditions may help for separation of the DNA strands for initiating of the replication process.

Now, let analyse the possible involvement of DNA read-out process in the cell cycle synchronization in eukariotes. We will not discuss here the

complex processes of cell cycle regulation in which the proteins are involved, but only the conditions of successful triggering and read-out of DNA. We may assume only that every individual cell possesses some kind of triggering mechanism. Such mechanism is necessary but not enough condition in order to initiate the read-out process. The DNA read-out can be successful only if conditions for emission of EM energy exist. Consequently it will depend of the following conditional states of DNA molecule:

(a) The two strands of one end of DNA must be separated (or unbalanced by promoter) in order the EM quanta (photons) to be emitted)

(b) The two strands (not counting the end conditions mentioned in (a)) must be completely symmetrical in order the read-out process to be self-sustainable.

The requirements (a) and (b) excludes the mRNA attachment to DNA or any other regulatory protein, so the transcription process and regulatory mechanisms should be completed. Then the optimum conditions for development of synchronized read-out as avalanche process should be the phase S (start of DNA replication).

Now let assume that the internal triggering mechanism provides triggering clocks with period much shorter than the cell cycle. They will not provide successful triggering until the conditions (a) and (b) are satisfied. However, once they are satisfied the DNA read-out will be successful. Then the emitted entangled photons with a large common energy and encoded sequence possess an increased probability for activation of similar read-out processes in the DNA of the neighbouring cells. The extremely fast read-out process could lead to similar read-out process in many DNA. In such case, the emitted entangled photons may additionally interfere and contribute to the avalanche process of synchronization. The avalanche process, however, will be contributed only of DNA molecules that do not have significant differences. In case of tissue and organ transplantation, the avalanche process will not work between the DNA from different species whose synchronization sequences are too different.

11.6.3. Environment considerations for the efficiency of the avalanche process

The phase accuracy of the cell cycle synchronization evidently depends of the individual cell cycle phases and environmental conditions.

11.6.3.1 Phase accuracy dependence of the cell cycle period

If considering the triggering of the synchronization from internal cell mechanism in a proper phase of the cell cycle, the period between two consecutive synchronization bursts will depend of the time lag between the local clock triggering events. Evidently the period of these events should be much smaller than the cell cycle period.

Let accept that the individual cell cycle regulation mechanisms provides a Gaussian type distribution of the cell cycle period from many cells. Then the optimum conditions for avalanche read-out should be expected in some moment that is closed but not overpassing the maximum of the Gaussian curve. Once it is initiated, the Gaussian curve will be cut down for all cell contributing to the avalanche. Those who had performed a preliminary read-out and those not activated by the synchronization will not contribute. The cells in which the transcription and regulation processes are not completed in this moment will also be excluded and their mitosis will not be in harmony with the synchronized cells.

Additionally we may not expect that all the synchronized cells will be activated in the very beginning of the read-out of the first activated cells. The repeatable sequences may provide conditions for larger number of entangled photons. Such photons posses also an increased probability for absorption and activation of similar repeats from DNA in other cells. **Consequently the probability for avalanche from tandemly repetitive sequences of DNA is larger.**

11.6.3.2 Physical factors of cell environment

The most important environmental factor for successful EM synchronization is the temperature.

It is reasonable to assume that the cascade energy transfer through the bonding path of the DNA strand is phase synchronized by the energy rotation

cycle in the (O+5C) rings. The duration of this cycle is:

$$T_R = t_O + 5t_C \qquad (3)$$

where: t_0 and t_c are respectively the lifetimes of the excited states in oxygen and carbon

The period, T_S, of the synchronization pulses is defined by the sum of the consecutive lifetimes through the bonding path of the strand, shown in Fig. 13

$$T_S = t_C + 5t_{av} \qquad (4)$$

where: t_{av} is the averaged lifetime value of the bonding electrons involved in the bonding path of the strand.

Then the condition for above mentioned phase synchronization is expressed by the relation:

$$T_S - T_R = t_0 - 4t_C - 5t_{av} = const \qquad (5)$$

The expression (5) is a constant for all involved DNA molecules if the same energy levels of the excited states are involved. This is a quantum mechanical condition that will depend only of the temperature. The successful generation of entangled photons, however, is additionally dependent of the correct spatial arrangement of the (2N+4C) rings. If the DNA molecule is sharply bent or it is in proximity to a protein involving magnetic field asymmetry, the condition of multiple photon entanglement will be disturbed. This will affect the efficiency of the synchronization process. Formations of Cruciforms, for example, may affect the emitted sequence. Z-type DNA inclusions and any external influences causing a helical non-uniformity of Beta type DNA may also block the successful read-out process.

The synchronization is possible in limited temperature range and good temperature uniformity along the DNA chain. The synchronization efficiency is dependent of the bending conditions of DNA and the spatial and helical uniformity along its chain. External factors causing any modification of the spatial parameters of the DNA double helix may inhibit the readout process.

11.7. Established features and experimental results supporting the hypothesis of the DNA involvement in the cell cycle synchronization

The proposed hypothesis is supported by a large number of established features of DNA molecules and experimental observations.

11.7.1 Absorption properties of DNA.

DNA absorbs ultraviolet light in the range of 240 to 280 nm with a maximum at about 260 nm. Increasing the temperature destabilizes the double helix. Experimental observation leads to a conclusion that the thermal stability of DNA is a function of base stacking, not only the hydrogen bonding (Saenger, 1984). This is in agreement with the suggested hypothesis of stabilizing magnetic field due to the cascade energy flow through the bonding paths of the DNA strands.

The mechanism of energy store and release suggested by the presented hypothesis is in agreement with the observations, reported by Joseph Lakowiccz et al. (2001) in a paper "Intrinsic Fluorescence from DNA can Be Enhanced by Metallic Particles". They use silver particles of size about 4 nm put in the surface of two quartz plates with distance between them of 1 - 1.5 um. The DNA placed in this gap has been excited at 287 nm with pulse sequence from dye laser with 100 ps pulse with. The intrinsic emission following such excitation in the range from about 330 to 350 nm is increased about 80 times around the metal particles. The detected radiation they believed to be from adenine and guanine.
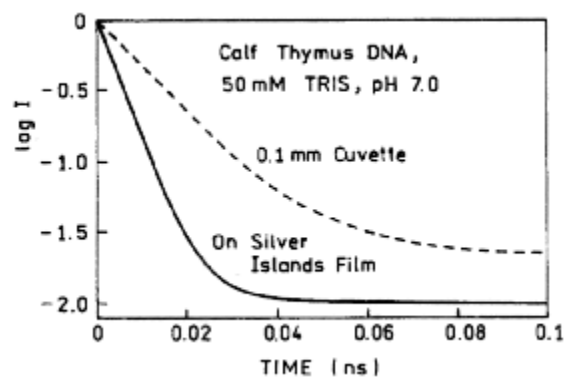

Fig. 21 Time-dependent intensity decay of DNA without metal (-) and between silver island film (Adapted from J. R. Lakowicz et al., 2001).

The authors explain the effect by a decreased lifetime in relation with the SERS effect (Surface-enhanced Ramman spectroscopy). Nevertheless, they also acknowledge the existence of another less understood effect. The obtained results of time dependent intensity decay are shown in Fig. 21 (corresponding to Fig 5 of their publication).

The explanation of the observed effect from a point of view of BSM theory and suggested hypothesis is a following. The laser pulse charges the energy storage rings of DNA. The silver metal islands introduce not uniformity field conditions in the proximity to DNA. In such conditions, the mechanism that may keep the stored energy in the rings is disturbed. Then a spontaneous read-out process may occur sooner in a case of DNA proximity of metal islands. This will appear in a shorter time interval between the excited pulse and the fluorescence emission in comparison to the case when DNA is not in proximity with such particles. This corresponds to the observed decreased lifetime. It is interesting to note that the fluorescence lifetime is still much longer than the lifetime in a single electronic bond. This means that the stored energies in the rings may have a number of rotational cycles.

11.7.2 Increased binding ability of some simple organic molecules

The proteins that bind to DNA are usually very large molecules containing thousands of atoms. But some comparatively simple organic molecules also have an increased ability for binding. When examining such molecules we see that they posses attached atomic rings. As was mentioned before, the energy in such rings is more stable. This gives them additional ability to interact with DNA based on magnetic field interactions. Such molecules for example are:

Trimethylpsoralen: 3 attached rings
Ethidium Bromide: 3 attached rings + 1 single
Chloroquine: 2 attached rings.

11.7.3 Effects of the salt concentration in helical winding and DNA supercoiling

As the concentration of a monovalent cation (Na^+) or divalent cation (Mg^{+2}) increases to high levels, the DNA double helix becomes wound less tightly.

According to the suggested hypothesis, the ion concentration influences the ion currents involved in the stabilisation of the magnetic field of DNA, responsible for its supercoiling shape.

11.7.4 Role of intermolecular triplexes in genetic recombination

Triplex DNA forming regions have been identified near sites involved in genetic recombinations. They usually have a mirror symmetry repeats of base pairs (as AGGAG). Kohwi and Panchenko (1993) found that the formation of intramolecular triplex structures in DNA in vivo can induce genetic recombination between two direct repeats flanking the triplex formed sequence.

According to the proposed hypothesis, the triplex formation in DNA disturbs the symmetry of the compensated field solenoid of DNA. Instead of flowing in the internal region of DNA, some of the magnetic lines are forced to pass through the external region. In conditions of chromosome recombination in vivo, the read-out process may be more often, than in the regulated cell cycle. Then the emitted sequence of entangled photons from one chromosome could be directly induced in the other. This may influence their common position and orientation. In the same time the magnetic field of the cascade energy transfer through the bonding path of the DNA strand is not compensated in the triplex region. When combining with a similar region from another chromosome the complex magnetic field may become compensated and stable.

11.7.5. Electronic properties of DNA

This subject is of increased interest of physicists and chemists. Despite the subject is far from new, it is very controversial. A recent overview paper about this topic is presented by C. Dekker in Physics World, 2001. The experimental results deviate from good insulator to good conductor, while many researchers consider that DNA is able to provide some kind of energy flows.

Currently two possible mechanism of charge transfer are accepted: a coherent process of single step electron tunnelling and a thermal hoping. It is interesting that a signature of cascade transfer ex-

ists in both suggested processes. While this theoretically suggested mechanisms seam reasonable, direct electrical measurements by number of physics groups provide conflicting results. The results reported by Hans-Werner Fink and Christian Schonenberger (1999), for 1 μm long DNA in vacuum indicate a good conductivity. However, this contradicts to the theoretical considerations where DNA is expected to behave as a semiconductor with a large energy gap between the valence and conduction bands. The experiments of Porath and co-workers (2000), for example, on a particular type of DNA - called poly(gG)-poly(dC) DNA and show that it behaves as a large gap semiconductor.

One important fact that may influence the experimental results is the different environmental conditions at which the experiments are performed. Additionally, in number of experiments the electronic properties are not directly measured, but derivable from the transient absorption spectra.

Let try to explain the possible electrical properties of DNA from the point of view of BSM models. In order to have a stable energy cascade transfer, the DNA must be in proper environments (pH, temperature, ATP) and to be enough long. In normal environments, it is considered a negatively charged. This charge, however, is uniformly distributed, so it may not influence the energy cascade transfer. In such case, the stored ring energies are synchronized and have a proper handedness. For small voltage along DNA, the electrons do not quit their spatially distributed orbits. For large voltages, however, the proximity proton field defining their orbits are biased, end the valence electron could jump synchronously. This transition, however, is expected to interact with the rotating energy states in the rings. The signature of such interaction might be the effect of "single step electron-tunnelling mechanism". It is evident that such conditions may occur only if a stable energy cascade transfer through the DNA strand exist, but the latter effect is possible only at proper environments.

12. Hypothesis of decoding process in some of the complexes aminoacyle-tRNA synthetases - tRNA.

12.1. General considerations and code analysis

The prototype of tRNA molecule is coded in the gene. The current estimate for number of tRNA in animals and plants is up to 50. The typical shape of the tRNA is shown in Fig. 16. The tRNA binds to the proper enzyme that charges to its end one of the 20 amino acids corresponding to the anticodon. Aminoacyl-tRNA Synthetase is a family of 20 enzymes whose structures are pretty well known. The enzyme usually recognize the corresponding tRNA using the anticodon.

Let analyse the coding of the amino acid by the anticodons used by tRNA. We may use for convenience the most popular RNA codons, shown in Table 12.1. Their number is 64. In a general case the anticodon code is directly obtainable from the corresponding codon code. One exclusion from that rule is the anticodon of Alanine, where the three codes GCU, GCC and GCA are presented by one codon CGI (I - Ionosine). This reduces the total number of anticodons to 61.

One feature of the amino acid coding, evident from the table, is the **code redundancy**. Most of the amino acids are coded by more than one codon. One additional surprise comes from the genome analysis. Some organisms don't have genes for all twenty aminoacyl-tRNA synthetases, but they still use all twenty amino acids to build their proteins.

The synthetase mechanism of the Aminoacyl-tRNA synthetases involves two steps. In the first step they form an aminoacyl-adenylate in which the carboxyl of the amino acid is linked to the alpha-phosphate of ATP by displacing pyrophosphate. In the second step, if only a correct tRNA is bound, the aminoacyl group of the aminoacyle-adenylate is transferred to 2' or 3' terminal OH of the tRNA.

Table 12. 1

UUU	Phenylalanine	UCU		UAU	Tyrosine	UGU	Cysteine
UUC		UCC	Serine	UAC		UGC	
UUA		UCA		UAA	Stop	UGA	Stop
UUG	Leucine	UCG		UAG	Stop	UGG	Tryptophan
CUU		CCU		CAU	Histidine	CGU	Arginine
CUC	Leucine	CCC	Proline	CAC		CGC	
CUA		CCA		CAA	Glutamine	CGA	
CUG		CCG		CAG		CGG	
AUU	Isoleucine	ACU		AAU		AGU	
AUC		ACC	Threonine	AAC	Asparagine	AGC	Serine
AUA		ACA		AAA		AGA	
AUG	Start; Methionine	ACG		AAG	Lysine	AGG	Arginine
GUU		GCU		GAU	Aspartic	GGU	
GUC	Valine	GCC	Alanine	GAC	acid	GGC	Glycine
GUA		GCA		GAA	Glutamic	GGA	
GUG		GCG		GAG	acid	GGG	

The second step is conditional. This means that if a wrong enzyme is bound to tRNA the output will be zero (not charging the proper amino acids). If assuming that the process of binding the correct complex of enzyme - tRNA is occasional, then the number of possible combination for all 20 amino acid codes is $2^{20} = 1048576$. This means such number of produced tRNA and enzymes, so it is unreasonable. Another possible option is the enzymes to recognize or at least to increase the probability to bind to the correct tRNA in which case the above number to be significantly reduced.

One of the currently discussed problems is how these enzymes (aminoacyle-tRNA synthetases) recognize 20 different flavours. It is estimated that they admit intrinsically small number of errors - about 1 in 10,000. The unmistakeably recognition of 20 different flavours looks as quite intelligent task for a biomolecular structure of only few thousands atoms.

The above task could not be resolved unless the enzymes have some sensors for preliminary detection before binding and some memory. Having in mind that the enzyme contains only a few thousands atoms it is apparent that such capability should be built very economically using some basic physical properties at atomic and molecular levels. Then the sensing should be based on some simplified detection mechanism of energy states, while the memory should be based on basic physical states of binary type. Let concentrate firstly on the memory feature. The possible binary physical states for a molecule of complexity of the enzymes are following:

(1) Quantum mechanical spin of the electron

(2) direction of magnetic field (S-N or N-S)

(3) handedness of rotating energy states (according to BSM)

(4) electrical charge (+ and -)

The option (4) could be excluded because its realization requires complex structure of semiconductor type. The most reasonable option is (3) with some combination of options (1) and (2).

Let evaluate the required memory for decoding the codon of any amino acid using the Boolean algebra without minimization. Any codon is a three-digit code. Anyone of these digits needs 4 states in order to present one of the four letters (A,B,C,D). Then the three-digit code of the codon could be presented of 12 bit binary code. This corresponds to a memory map of 4096 bits. Such memory hardly be achieved by any enzyme whose molecule usually includes a few thousands atoms. Additionally the enzyme must have remote sensors for recognition of tRNA before binding and tools for test of the anticodon.

Obviously, the above general approach for decoding of 20 flavours is not feasible. We must look for some economic natural code hidden in the codons and particularly behind their redundancy.

Let analyse the redundancy using some of the unveiled properties of the ring structures and the possibility for detection of their type. The Purines are distinguishable from the Pyrimidines by the number of rings (able to carry different stored energies), so they could be sensed by some kind of binary test. The possible mechanism of such test will be discussed later. In order to see, how such consecutive tests of the first, second and third letter of the codon will lead to some results, we make the following substitution for the codons in Table 12.1.

      Purines (A and G)   -> 2
      Pyrimidines (C and U) -> 1

The digits 1 and 2 in this substitution in fact correspond to the number of the atomic rings.

Table 12.2

111	111	121	121
111	111	121	121
112	112	122	122
112	112	122	122
111	111	121	121
111	111	121	121
112	112	122	122
112	112	122	122
211	211	221	221
211	211	221	221
212	212	222	222
212	212	222	222
211	211	221	221
211	211	221	221
212	212	222	222
212	212	222	222

Table 12.2 shows the obtained codes after this substitution. This table does not contain the names of the amino acids, but they are identifiable by the code positions. When examining the Table 12.2 we see that binary codes (expressed by 1 and 2) are in very strict order.

Let find out how many aminoacids every code from the Table 12.2 is related to. The result is shown in Table 12.3

Table 12.3

Code from Table 12.2	No of coded amino acids	Additional coding
111	4	
112	4	
121	4	
122	3	stop
211	4	
212	5	start
221	4	
222	4	

Table 12.3 shows a pretty uniform distribution of the amino acid codes based on the distinguishing features between the Purines and Pyrimidines. Only the codes for start and stop deviate from the uniformity of the distribution. From this simple analysis, however, one useful conclusion could be made:

The number of possible combinations could be significantly reduced if initial binary detection of Purines or Pyrimidines is performed.

The Purines and Pyrimidines are distinguishable by the number of rings. It will be described later that their possible remote detection have some similarity with the process of DNA readout described in section 11.6.

Let denote the tRNA anticodon by the triplet *abc*, but using instead the corresponding codons of RNA. The following example shows the reduction of the possible combinations in three consecutive binary tests (Purines or Pyrimidines) applied for the codes of Table 12.2. Let the first test for *a* gives value: *a* = 1. This means that all codons starting with 2 are excluded from the following tests, while those starting with 1 are enabled. Only 32 from of all 64 combinations are left. This is illustrated in Table 12.4., where the excluded combinations are masked by a grey colour.

a = 1   **Table 12.4**

111 111 112 112	111 111 112 112	121 121 122 122	121 121 122 122
111 111 112 112	111 111 112 112	121 121 122 122	121 121 122 122
211 211 212 212	211 211 212 212	221 221 222 222	221 221 222 222
211 211 212 212	211 211 212 212	221 221 222 222	221 221 222 222

c = 2   **Table 12.6**

111 111 112 112	111 111 112 112	121 121 122 122	121 121 122 122
111 111 112 112	111 111 112 112	121 121 122 122	121 121 122 122
211 211 212 212	211 211 212 212	221 221 222 222	221 221 222 222
211 211 212 212	211 211 212 212	221 221 222 222	221 221 222 222

Let apply the same test for b and the result for example is b = 2. The available combinations are additionally reduced in half as shown in Table 12.5.

b = 2   **Table 12.5**

111 111 112 112	111 111 112 112	121 121 122 122	121 121 122 122
111 111 112 112	111 111 112 112	121 121 122 122	121 121 122 122
211 211 212 212	211 211 212 212	221 221 222 222	221 221 222 222
211 211 212 212	211 211 212 212	221 221 222 222	221 221 222 222

In a similar way the third test of c, for example, with a result *c* = 2 will lead to reduction of the available combinations to 8 as shown in Table 12.6.

We see that by three consecutive tests the available combinations are reduced from 64 to 8, while they address only 4 amino acids. If assuming that this test is performed prior to binding of the enzyme to the tRNA, then the required combinations for a probable correct match are only $2^4 = 16$. Consequently a possible remote sensing will reduce the amount of the necessary number of enzymes and tRNA by a factor of 65536.

The additional tests for identification of the correct amino acids require distinguishing of Adenine from Uracile and Guanine from Cytozine for every letter of the triplet *abc*. The detection for such identification, however, could not be remote and perhaps is performed in the second step of the synthetase mechanism. It is known, for example, that in glutaminyl-tRNA synthetase with its tRNA the enzyme firmly grips the anticodon, spreading the three bases widely apart. Let assuming that the enzyme keeps in its memory the binary results of the previous remote detection (Purines or Pyrimidines) for every letter. Then the following test after the enzyme has grabbed the anticodon (for every letter of the codon) must be also a binary test of a type: Adenine (A) or Guanine (G) and Cytozine (C) or Uracile (U). How they could be distinguished, while they have the same number of rings? When examining their structure we see that the larger ring of Adenine includes three bonds of

single valence, while the larger ring of Guanine includes four bonds of single valence. The ring of Cytosine includes two bonds of second valence, while the ring of Uracile includes one bond of second valence. These differences of the ring structures may cause significant differences in their spectral emission-absorption capability. The very narrow temperature range will define a pretty narrow range of the population of the excited states. This may simplify the task for recognizing the differences between (A and G) and (C and U) by their spectral signatures.

After all these binary tests are performed, it seems that the correct amino acid should be decoded. However, we must not forget that the letters *abc* must be read in a correct order (most significant and less significant digit). If this rule is not observed the following code misinterpretation may occur:

UUA	confused with	AUU
UUC	-	CUU
UUG	-	GUU
UCC	-	CCU
CCA	-	ACC
AAG	-	GAA
UGG	-	GGU

Assuming that the memory map of the enzyme is naturally minimized, the correct code readout obviously must be initially detected prior to the remote sensing described above. In order to find out the possible detection mechanism for the correct code readout direction, we may examine the structure of tRNA that has been already shown in Fig. 16. In the left side of the figure, the real shape of the backbone structure is shown. In the right side of the same figure, the tRNA is presented like a flat curve in order to show more clearly some of its structural features such as, the folding of the single strand in cloverleaf shape, the position of loops, the H-bonds, the position of the anticodon and the asymmetrical ends.

The tRNA strand is similar as the DNA strand and contains regularly attached (O+4C) rings. In proper environment the tRNA could be energized, so a cascade energy transfer may occur through its strand in a similar way as in the DNA and proteins. The asymmetrically terminated end of tRNA may assure the proper direction of the cascade energy transfer. If such process is stable enough for a short

time, the rotating energies in (O+4C) rings can be synchronized, obtaining in such way a proper handedness. The same is valid for the H-bonding base pairs and consequently for the codon loop. While the tRNA is not so long (75 - 90 nucleotides) the energy cascade process could not be so stable like in the DNA and the proteins. The disruption of the energy cascade will lead to synchronized readout of the rotating energy states in (O+4C) rings that could be emitted as a coherent sequence of photon pulse whose parameters (phase sequence) will carry the direction of codon readout. This readout of (O+4C) energies from its side might provoke a readout process from the base pairs in a similar way as in the DNA. The conditions for emission from tRNA, however, are different from those of DNA due to the different shape of the tRNA molecule. Let assuming a hypothetical axis (not exactly linear), defined by the twisting shape (known as a secondary structure) of tRNA and passing from the anticodon loop of tRNA to its terminating ends. The two major side loops of tRNA could be regarded as approximately symmetrical pairs in respect to the introduced axis. The supercoiling and tertiary structure may also influence the symmetry of the mentioned pairs, but will not influence the symmetrical features of the anticodon loop. In the same time, all the loops are free of H-bonds. If regarding the emission process as EM filed, it is evident that the two side loops are complimentary and will have a comparatively smaller EM emission capability (because the magnetic lines appears closed in a circle around the introduced tRNA axis). The anticodon loop, however, does not have complimentary symmetry with another loop, so its emission capability could be much larger. Then the emitted photons from the anticodon loop could be detected remotely by the correct enzyme. The burst of photon sequence from (O+4C) rings readout may serve as a synchronization that prepares the enzyme for detection of the anticodon. In such process the detection could be of synchronized type, so it could allow an increased probability for detection of the anticodon sequence. The tRNA could be re-energize and the readout sequence could be performed a few times. In such way, the anticodon could be detected by number of corresponding enzymes.

The remotely detected sequence from antico-don loop (carrying information for Purines or Pyrimidines) could be regarded as very fast consecutive tests of the letters in the triplet *abc* prior to binding of the correct enzyme to tRNA. The test results, however, will be additionally needed for the consecutive tests (A or G and C or U) that will be performed after the binding of the enzyme to tRNA. Let assuming that these test results are directly passed to some kind of binary decoder implemented in the enzyme. Then after this remote test the

number of codons from 64 is reduced to 8, corresponding to 4 amino acids. This significantly increases the probability of correct binding between tRNA and the corresponding enzyme.

12.2 Decoding algorithm

Fig. 22 presents the decoding algorithm according to the analysis and considerations discussed in the previous paragraph.
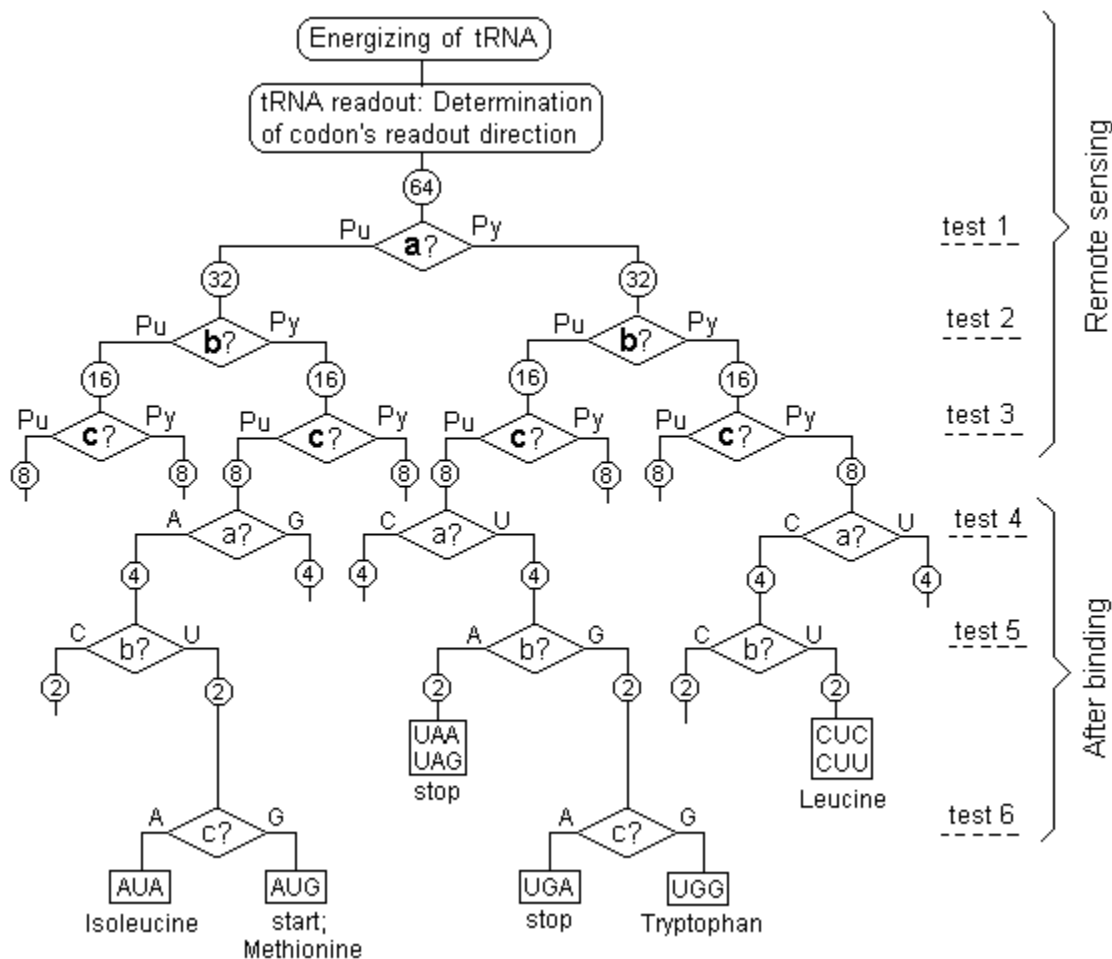

Fig. 22. Decoding algorithm according to the hypothesis of decoding process in some of the complexes tRNA - enzyme.

The remote sensing includes tests 1, 2, 3, while the other tests are performed after the tRNA is bound to the correct enzyme. The numbers in circle show the enabled codon combinations after each test. Not all the decoding tree is shown, but the algorithm for a possible decoding of all 20 aminoacids is the same. It is evident, that maximum of 6 tests are necessary for decoding of anyone of the aminoacids, but some of them are decoded even at

test No 5. (Leucine, for example). Two of the stop codons are also decoded at test No. 5. This provides the opportunity to use the test No. 6 for additional true test, that should increase the decoding reliability. The other stop codon UGA, however is decoded after the test No. 6. Then it could be interesting to study the statistics of UAA and UAG stop codons in comparison with the UGA stop codon (in both the RNA and DNA sequences).

According to the suggested algorithm, the tests from the remote sensing increase the probability for correct binding between tRNA and the proper enzyme, but does not exclude completely wrong bindings. It is logical to expect that only a correct binding will lead to attachment of amino acid after the tests 3, 4 and 5. The wrong binding will provide a zero result.

Discussion.

The reader of this article who has not been acquainted with the BSM theory may put one reasonable question: Why the suggested atomic models, pretending to match the physical reality, are not firstly officially promoted by the theoretical physics? The answer is: The derived atomic models are result of a new concept about the space, known as a vacuum. This is of fundamental aspect for the theoretical physics. In the present time when a large number of highly abstractive and mathematically sophisticated theories are developed, any change of fundamental physical aspect may lead to more or less painful process of adaptation in different fields. In such aspect the official promotion for a radical change might be delayed for years. In the fields of structural chemistry and molecular biology, however, the suggested physical models of atoms could be applied without waiting for such a long period. The presently known three-dimensional structures of the biomolecules possess enough information for reliable validation of the suggested atomic models. In the same time, the using of these models in the analysis of the experiments may lead to new discoveries about the properties of the biomolecules.

The Quantum mechanical models of the atoms are very useful for their ability to provide accurate calculation of the energy levels and interaction probabilities. The models, suggested by BSM theory, do not intend to replace or undermine the useful features of the quantum mechanical models but to enrich the knowledge about the physical structures of the atoms and the quantum processes at subatomic level.

Acknowledgement

References:

C. B. Anfinsen, J, T. Edsall and F. M. Richards, Advances in protein chemistry, vol. 34, 1981, Academic Press.

I. Dabrowski, Can. J. Phys. 62, 1639 (1984)

C. Dekker, Physics World, Aug. 2001

H-W Fink and C. Schonenberger, Electrical conduction through DNA molecule, Nature, **398**, 407, (1999)

W. M. Gelbart, R. F. Bruinsma, P. A. Pincus and V. A. Parsegian, DNA-inspired electrostatics, Physics Today, 38-44, (2000).

K. Kimura et al., Handbook oh He I PE Spectra of Fundamental organic molecules, Japan Scientific Societies Press (1981)

Y. Kohwi and Y. Panchenko, Transcription-dependent recombination induced by triple-helix formation. Genes Dev. 7, 1766-1778, (1993)

J. R. Lakowicz, B. Shen, Z. Gryczynski, S. D'Auria and I. Gryczynski, Intrinsic fluorescence from DNA can be enhanced by metalic particles, Biochemical and Biophysical Res. Comm., 286, 875-879 (2001)

D. Porath et al., Direct measurement of electrical transport through DNA molecules, Nature, **403**, 635, (2000)

W. Saenger, "Principles of Nucleic Acid Structure", Springer-Verlab, Ney York, (1984)

S. Sarg, "Basic Structures of Matter", thesis, (2001),
http://www.helical-structures.org
also in:
http://collection.nlc-bnc.ca/amicus/index-e.html
(AMICUS No. 27105955)

S. Sarg, Atlas of Atomic Nuclear Structures (2001)
http://www.helical-structures.org
also in:
http://collection.nlc-bnc.ca/amicus/index-e.html
(AMICUS No. 27106037)